

# Numerical investigations of the effect of operation conditions on the heat transfer of the supercritical water in the Canadian SCWR fuel bundle

Huirui Han, Chao Zhang\*

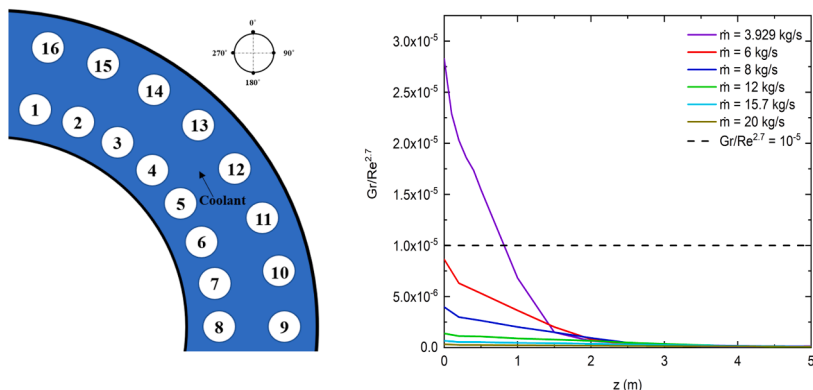
Department of Mechanical & Materials Engineering Western University, 1151 Richmond Street, London, ON, N6A 5B9 Canada



## HIGHLIGHTS

- The heat transfer of the supercritical water in the fuel bundle at different operation conditions was investigated.
- Criteria of the onset of buoyancy effect on the heat transfer deterioration were evaluated.
- The buoyancy-affected zone mainly exists at the region where the bulk temperature is close to the pseudocritical temperature.

## GRAPHICAL ABSTRACT



## ARTICLE INFO

### Keywords:

Heat transfer  
Supercritical water  
Fuel bundle  
Wall temperature  
Buoyancy effect

## ABSTRACT

The safety of the nuclear reactor depends on the heat transfer of the supercritical water in the fuel bundle. Investigations of effects of operating conditions on the heat transfer of the nuclear reactor are still lacking. In this study, the effects of the operating pressure, inlet temperature, heat flux, and mass flux on the heat transfer of upward supercritical water flow in the 64-element fuel bundle were studied numerically. The criteria of the onset of buoyancy effect on the heat transfer deterioration in circular tubes were also used to evaluate the buoyancy effect on the heat transfer in the fuel bundle. The results show that the wall temperature generally increases with the increase in the inlet temperature, heat flux, or the decrease in the mass flux. The buoyancy-affected zone mainly exists at the pseudocritical temperature region and it will disappear when the mass flux is above a certain value.

## 1. Introduction

Supercritical water was first considered as the working fluid in the concept of the supercritical fossil-fueled power plants in the 1950s. Later

in the 1960–1970s, some early studies were conducted to find the possibility of the supercritical water used in nuclear reactors [1–5]. The thermophysical properties of the supercritical water undergo significant changes within around  $\pm 25\text{C}$  in the vicinity of the pseudocritical temperature. Fig. 1 shows the variations of thermophysical properties of

\* Corresponding author.

E-mail addresses: [hhan55@uwo.ca](mailto:hhan55@uwo.ca) (H. Han), [cchang@eng.uwo.ca](mailto:cchang@eng.uwo.ca) (C. Zhang).

Nomenclature	
<i>Symbols</i>	
$\text{Bo}^*$	Dimensionless parameter, $\text{Bo}^* = \text{Gr} / (\text{Re}^{3.425} \text{Pr}^{0.8})$ .
$c_p$	Specific heat, J/kg•K.
$D$	Diameter of the tube, m.
$g$	Gravitational acceleration, m/s <sup>2</sup> .
$G$	Mass flux, kg/m <sup>2</sup> •s.
$\text{Gr}$	Grashof number.
$\dot{m}$	Mass flow rate, kg/s.
$P$	Pressure, Pa.
$\text{Pr}$	Prandtl number.
$q$	Heat flux, W/m <sup>2</sup> .
$\text{Re}$	Reynolds number.
$T$	Temperature, °C.
$u$	Velocity, m/s.
$x_i$	Position vector.
$y^+$	Nondimensional distance from the wall, $y^+ = \frac{u_i y}{v}$ .
$z$	Axial location, m.
<i>Greek letters</i>	
$\theta$	Circumferential degree.
<i>Subscripts</i>	
$b$	Bulk.
$in$	Inlet.
$o$	Operating point.
$pc$	Pseudocritical.
$t$	Turbulent.
$w$	Wall.
<i>Superscript</i>	
$\overline{\cdot}$	Reynolds averaged.
<i>Acronyms</i>	
DHT	Deteriorated Heat transfer.
NIST	National Institute of Standards and Technology.
RSM	Reynold Stress Model.
SCWR	Supercritical Water-Cooled Reactor.
SIMPLEC	Semi-Implicit Pressure-Linked Equations-Consistent.

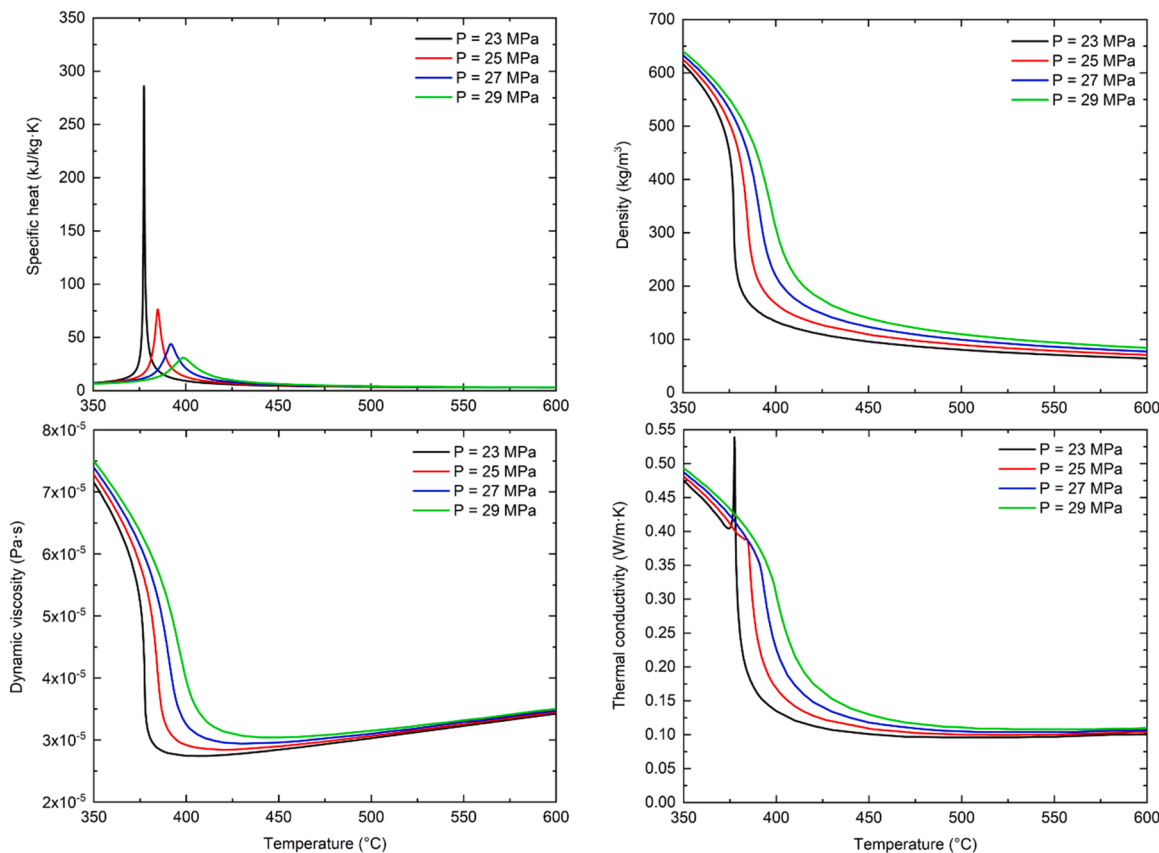


**Fig. 1.** Thermophysical properties of water at supercritical pressures [6].

the supercritical water versus temperatures at different pressures [6]. The specific heat increases first and then decreases with the increase in the temperature. The temperature corresponding to the peak value of the specific heat is the pseudocritical temperature. The pseudocritical temperatures and corresponding peak values of the specific heat at different pressures are presented in Table 1. At a given temperature, the

fluid with a higher specific heat absorbs more heat. It is found that the pseudocritical temperature increases with the pressure while the maximum value of the specific heat decreases with the increase of the pressure. Similar variations of density and thermal conductivity are observed. The density and thermal conductivity decrease with the increase of the temperature and the gradient of the reduction is relatively

**Table 1**

Pseudocritical temperatures and corresponding peak values of the specific heat at different pressures [6].

Pressure (MPa)	Pseudocritical temperature (°C)	Peak value of specific heat (kJ/kg·K)
23	377.5	284.3
25	384.9	76.4
27	392.0	43.9
29	398.7	30.9

large near the pseudocritical temperature. The density decrease could increase the effects of the buoyancy force and the flow acceleration. In addition, the reduction of the thermal conductivity would also impair the heat transfer. Generally, the density and thermal conductivity increase with the pressure. However, there is a peak in the thermal conductivity near the pseudocritical temperature when the pressure,  $P = 23 \text{ MPa}$ , which is similar to the peak in the specific heat at the same pressure. But there are no peaks in the thermal conductivity at other pressures. The dynamic viscosity decreases with the increase in the temperature when the temperature is less than 400–410°C. Near the pseudocritical point, the dramatic decrease of the viscosity could lead to a significant increase in the velocity of the fluid and the Reynolds number. It is also shown that the dynamic viscosity slightly increases with the increase in the temperature before the pseudocritical points. When the temperature is higher than the pseudocritical temperatures, the viscosities at different pressures gradually increase and become almost the same after 500°C. All of the variations of the thermophysical properties listed above results in different heat transfer characteristics of supercritical water at various operating conditions.

The supercritical water-cooled reactors (SCWRs) were proposed as one of the six Generation IV nuclear reactors since 2002 [7], which have regained researchers' interest in the heat transfer characteristics of the water at supercritical pressures. Many experimental and numerical studies.

have been devoted to the heat transfer of supercritical water in different flow channels, including horizontal and vertical tubes, and rod bundles. Three types of heat transfer regimes could occur: normal heat transfer, deteriorated heat transfer, and enhanced heat transfer [6, 8–11]. According to these studies, several operating parameters found

influence the heat transfer of the supercritical water in channels, such as operating pressure, inlet temperature, heat flux and mass flux, heat to mass flux ratio. The heat transfer deterioration mostly exists at high heat fluxes or low mass fluxes conditions. In the existing studies of the supercritical water in the horizontal tubes [5,12–14], the results generally showed that there are large differences between the top and bottom wall temperatures. This can be explained by the buoyancy effect due to the significant decrease of the density in the near wall region. In the present study, the investigations of heat transfer of the supercritical water in vertical channels will be carried out.

At a supercritical pressure, the dynamic viscosity and thermal conductivity are higher at higher operating pressures. The experiment results [15–17] indicated that the heat transfer coefficient generally increases with the decrease in the pressure when other operating parameters are kept constant. However, contrary results were also observed by Gang et al. [18]. Their results showed that the heat transfer coefficient increased with the increase in the pressure when the mass flux,  $G = 350 \text{ kg/m}^2\cdot\text{s}$  while decreased with the increase in the pressure when  $G = 1000 \text{ kg/m}^2\cdot\text{s}$ . This opposite trend was assumed due to the heat transfer deterioration occurring at  $G = 350 \text{ kg/m}^2\cdot\text{s}$  when the

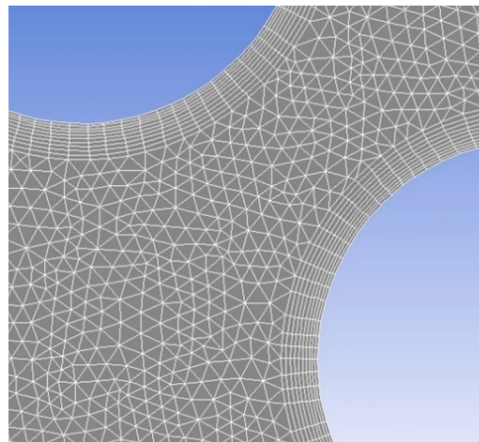


Fig. 3. Near wall mesh.

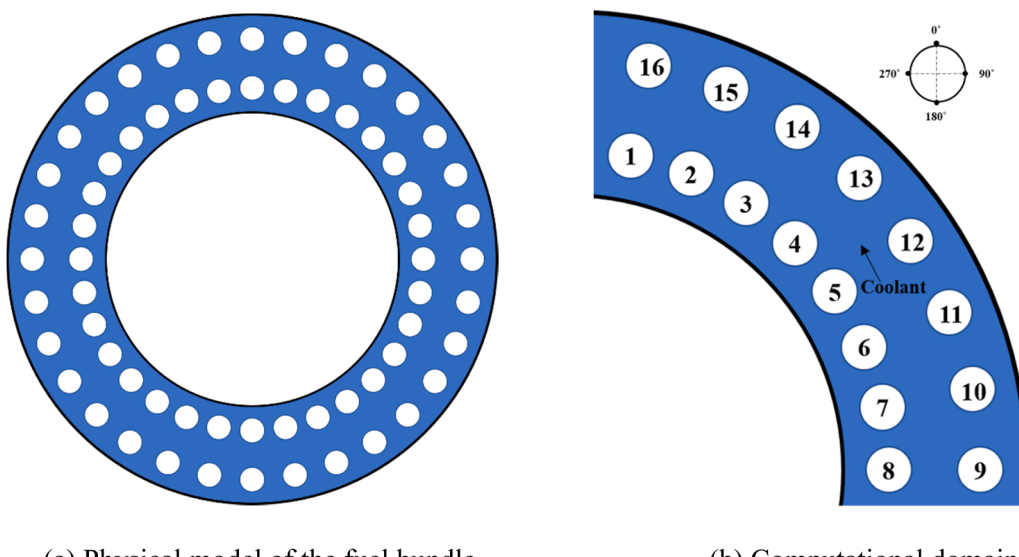
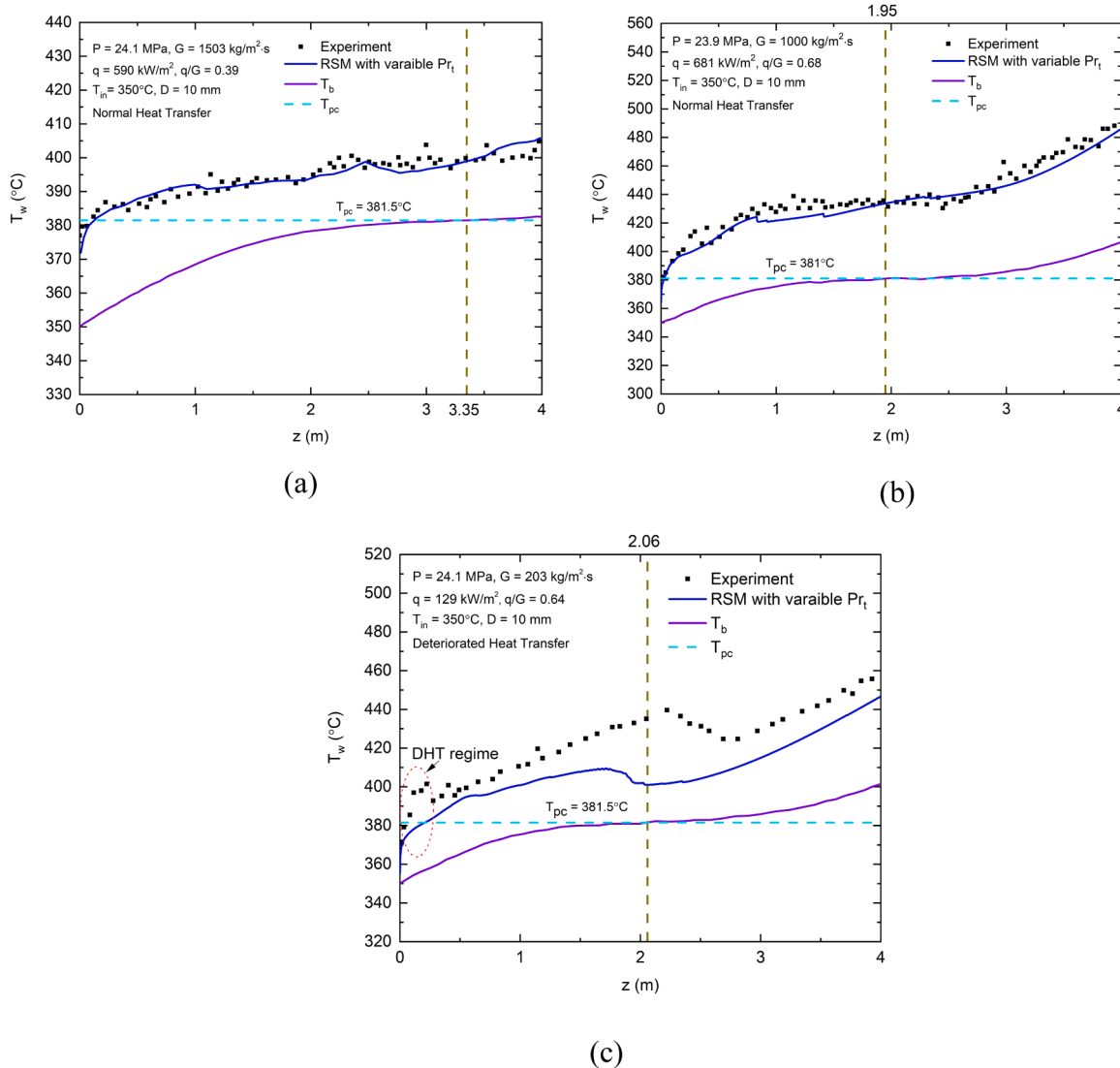


Fig. 2. Cross- section view of the fuel bundle.

**Table 2**

Operating parameters for different cases.

Case #	P (MPa)	Normalized P	$T_{in}$ (°C)	Normalized $T_{in}$	q (kW/m <sup>2</sup> )	Normalized q	$\dot{m}$ (kg/s)	Normalized $\dot{m}$	Heat to mass flux ratio
1	25	$P_o$	350	$T_{in,o}$	879.93	$q_o$	3.93	$\dot{m}_o$	1.02
2	23	0.92 $P_o$	350	$T_{in,o}$	879.93	$q_o$	3.93	$\dot{m}_o$	
3	27	1.08 $P_o$	350	$T_{in,o}$	879.93	$q_o$	3.93	$\dot{m}_o$	
4	29	1.16 $P_o$	350	$T_{in,o}$	879.93	$q_o$	3.93	$\dot{m}_o$	
5	25	$P_o$	340	0.97 $T_{in,o}$	879.93	$q_o$	3.93	$\dot{m}_o$	
6	25	$P_o$	360	1.03 $T_{in,o}$	879.93	$q_o$	3.93	$\dot{m}_o$	
7	25	$P_o$	370	1.06 $T_{in,o}$	879.93	$q_o$	3.93	$\dot{m}_o$	
8	25	$P_o$	350	$T_{in,o}$	600	0.68 $q_o$	3.93	$\dot{m}_o$	0.70
9	25	$P_o$	350	$T_{in,o}$	700	0.80 $q_o$	3.93	$\dot{m}_o$	0.81
10	25	$P_o$	350	$T_{in,o}$	800	0.91 $q_o$	3.93	$\dot{m}_o$	0.93
11	25	$P_o$	350	$T_{in,o}$	879.93	$q_o$	6	$1.53\dot{m}_o$	0.67
12	25	$P_o$	350	$T_{in,o}$	879.93	$q_o$	8	$2.04\dot{m}_o$	0.50
13	25	$P_o$	350	$T_{in,o}$	879.93	$q_o$	12	$3.05\dot{m}_o$	0.33
14	25	$P_o$	350	$T_{in,o}$	879.93	$q_o$	15.7	$3.99\dot{m}_o$	0.26
15	25	$P_o$	350	$T_{in,o}$	879.93	$q_o$	20	$5.09\dot{m}_o$	0.20

**Fig. 4.** Comparison between the simulation results and experimental data for the supercritical water flow in a bare tube.

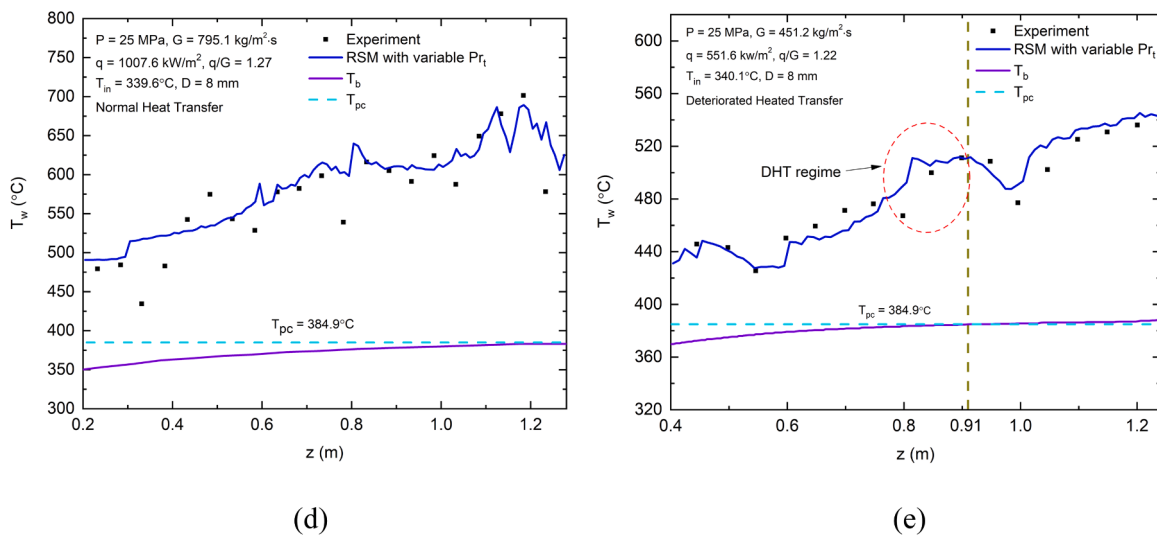


Fig. 5. Comparison between the simulation results and experimental data for the supercritical water flow in a rod bundle.

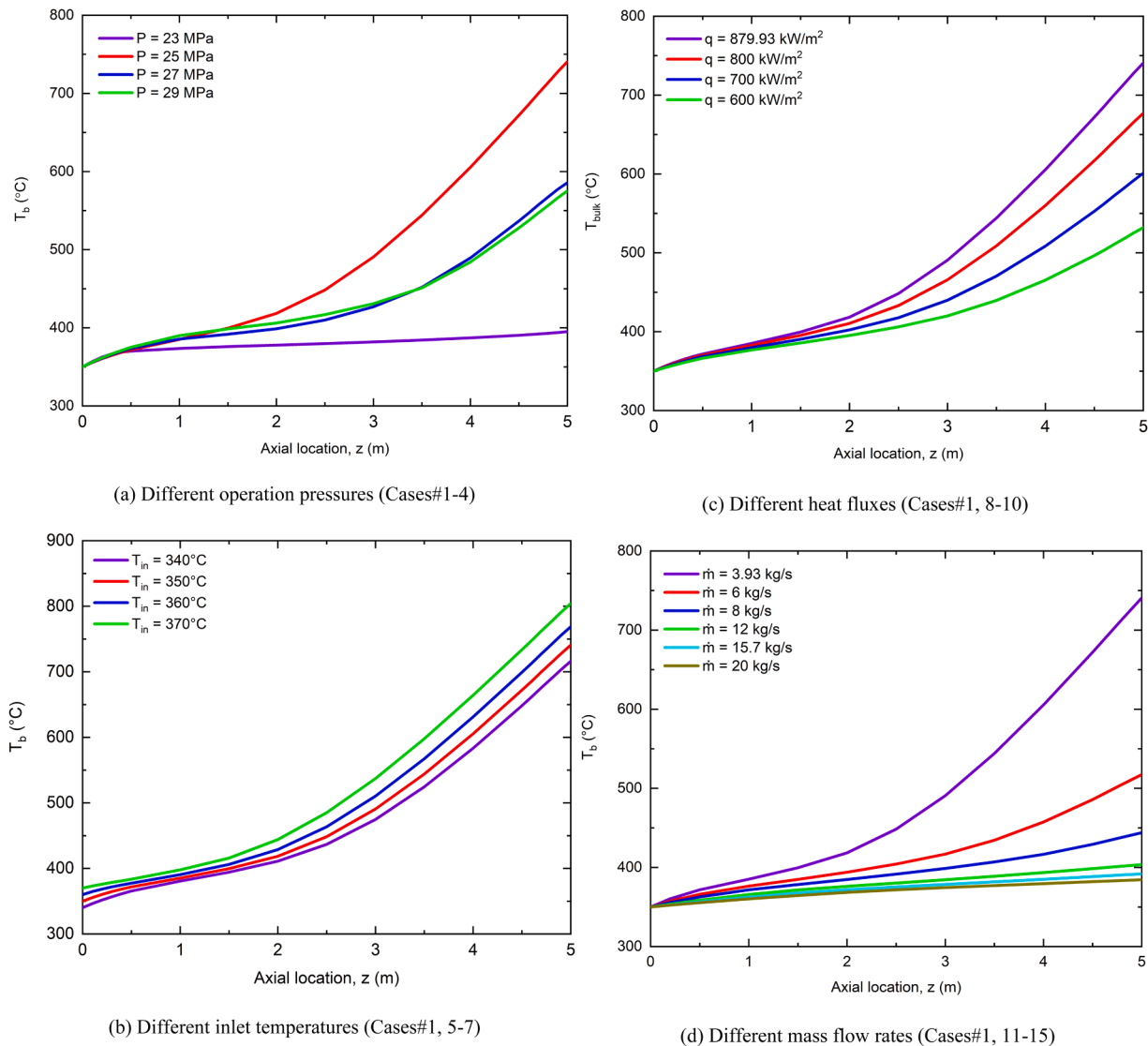
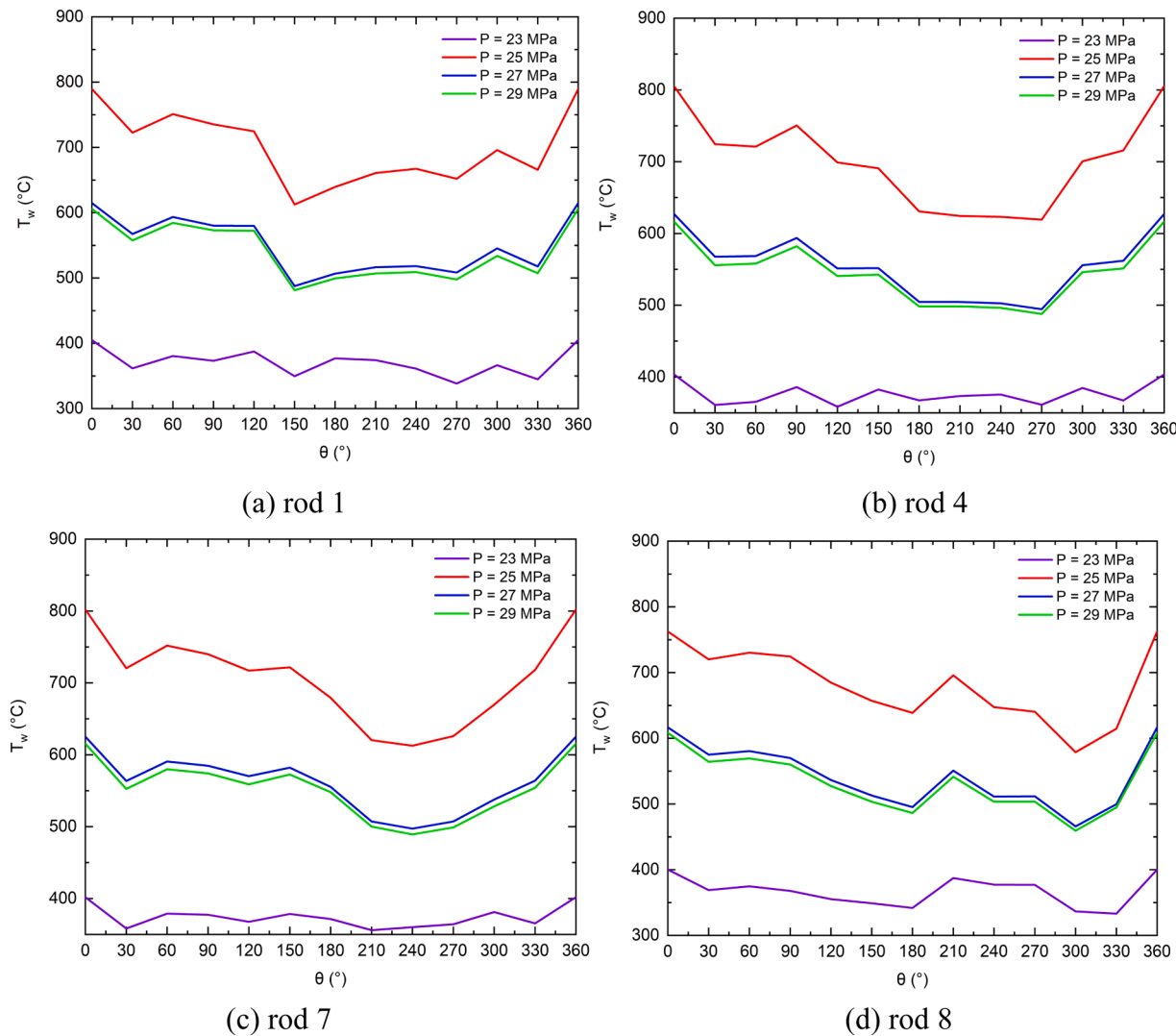


Fig. 6. Comparisons of the bulk temperature distributions along the axial direction at different operating conditions.



**Fig. 7.** Circumferential wall temperature distributions at  $z = 4.8$  m under different operating pressures.

operating pressure,  $P = 23$  MPa. Some researchers [18–20] claimed that the heat transfer coefficient would increase with the pressure when the heat to mass flux ratio is relatively high. In such condition, the heat transfer deterioration due to the buoyancy effect prevails over the heat transfer enhancement by the pressure changes. There are limited studies on the effects of the inlet temperature on the heat transfer of supercritical fluids in channels [21,22]. The investigations on the heat transfer phenomenon of supercritical water in the rod bundles conducted by Podila et al. [21] indicated that the increase of the inlet temperature could effectively restrain the occurrence of the heat transfer deterioration.

The effects of heat flux on the heat transfer of the supercritical water in channels were investigated by several researchers [5,12,15,18,19, 23–25]. In these studies, the influence of the heat flux on the heat transfer was investigated at different bulk fluid temperatures and the wall temperatures. When the heat flux rises, both the fluid temperature and wall temperature would go up accordingly. When the fluid temperature is near the pseudocritical temperature, the sharp increase of the specific heat and decrease of viscosity and density could enhance the heat transfer. On the other hand, when the wall temperature is higher

than the pseudocritical temperature, the density, thermal conductivity, and specific heat of the fluid near the wall could be much lower, which in turn deteriorate the heat transfer between the wall and the fluid. With a relatively lower heat flux, the enhanced effect on the heat transfer contributed from the fluid temperature overwhelms the deteriorated effect on the heat transfer caused by the wall temperature when the fluid temperature is near the pseudocritical temperature and wall temperature is slightly high than the pseudocritical temperature. Conversely, at relatively high heat flux condition, the deteriorated effect on the heat transfer due to the wall temperature prevails over the enhanced effect on the heat transfer caused by the fluid temperature when the fluid temperature is near or slightly higher than the pseudocritical temperature and wall temperature is appreciably higher than the pseudocritical temperature. In addition, the effects of buoyancy and flow acceleration due to the significant density drop are more obvious at a higher heat flux. This further makes the effects of heat flux on the heat transfer of the supercritical water in channels more complicated.

The effects of the mass flux on the heat transfer of the supercritical water in channels were investigated by several researchers [14,25–28, 30,31–33]. Generally, under a relatively high mass flux condition, the

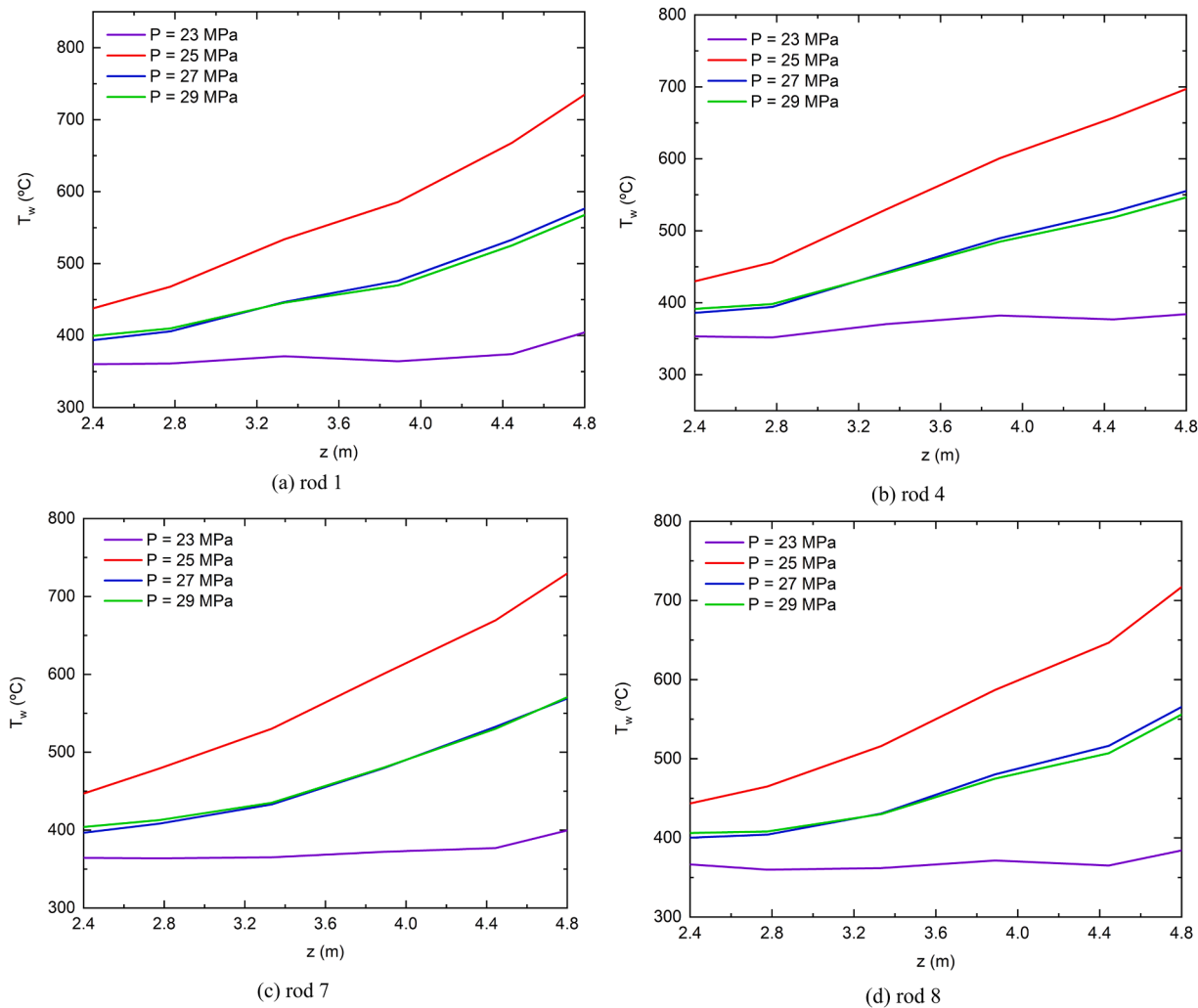


**Fig. 8.** Wall temperature distributions along the axial direction under different operating pressures.

heat transfer is improved with the increase in the mass flux. However, under a low mass flux condition, the heat transfer is found impaired with the increase in the mass flux. In the investigations on the heat transfer of the supercritical water in an inclined upward tube by Yin et al. [34], they found that the wall temperature at the top of the cross section decreased with the increase in the mass flux. However, the wall temperature at the bottom of the cross section increased with the increase in the mass flux ( $G = 600\text{--}900 \text{ kg/m}^2\cdot\text{s}$ ) at first and then decreased with further increase in the mass flux ( $G = 1200 \text{ kg/m}^2\cdot\text{s}$ ). Therefore, the effect of the mass flux on the heat transfer of the supercritical water in channels is different for high and low heat flux. Many efforts were made to use the heat to mass flux ratio ( $q/G$ ) to determine the criterion for the prediction of the onset of the heat transfer deterioration [24,29,31,35, 36]. Some researchers proposed the occurrence of the heat transfer deterioration when the heat flux to the mass flux ratio,  $q/G > 0.6\text{--}0.9 \text{ kJ/kg}$  within the range of  $G = 310\text{--}1830 \text{ kg/m}^2\cdot\text{s}$  and  $P = 22.5\text{--}29.4 \text{ MPa}$  and others proposed  $q/G > 0.81\text{--}1.21 \text{ kJ/kg}$  at  $P = 22.5\text{--}29.4 \text{ MPa}$  for the onset of the heat transfer deterioration. There are obvious differences in the proposed heat to mass flux ratio for the heat transfer deterioration in the literature. Therefore, a simple heat to mass flux ratio might not be able to exactly represent the onset of the heat transfer deterioration since the complicated heat transfer of the supercritical water in channels under different operating conditions.

Existing studies on the effects of different operating parameters on the heat transfer of the supercritical water in channels mainly focus on the tube flows. One study was for a  $2 \times 2$  rod bundle [27]. Because of the difference of the geometry in heated surface, the results from existing studies on the heat transfer of the supercritical water in simple channels cannot be regarded directly applicable in the fuel bundle in engineering applications. In this study, the investigations of the effects of various operating parameters, including the operating pressure, inlet temperature, heat flux, and mass flux on the heat transfer of the supercritical water in the 64-element fuel bundle in the Canadian SCWR were conducted. In addition, the buoyancy effect on the heat transfer at under different operating conditions was also evaluated.

## 2. Numerical model

### 2.1. Physical model and boundary conditions

To investigate the heat transfer characteristics of the supercritical water in the fuel bundle, numerical simulations are conducted in the present study. The cross-section views of the physical model of the fuel bundle and the computational domain used in the simulation are shown in Fig. 2. The rod bundle design used in this work consists of 64 fuel rods, which are arranged in a two-ring configuration with 32 elements

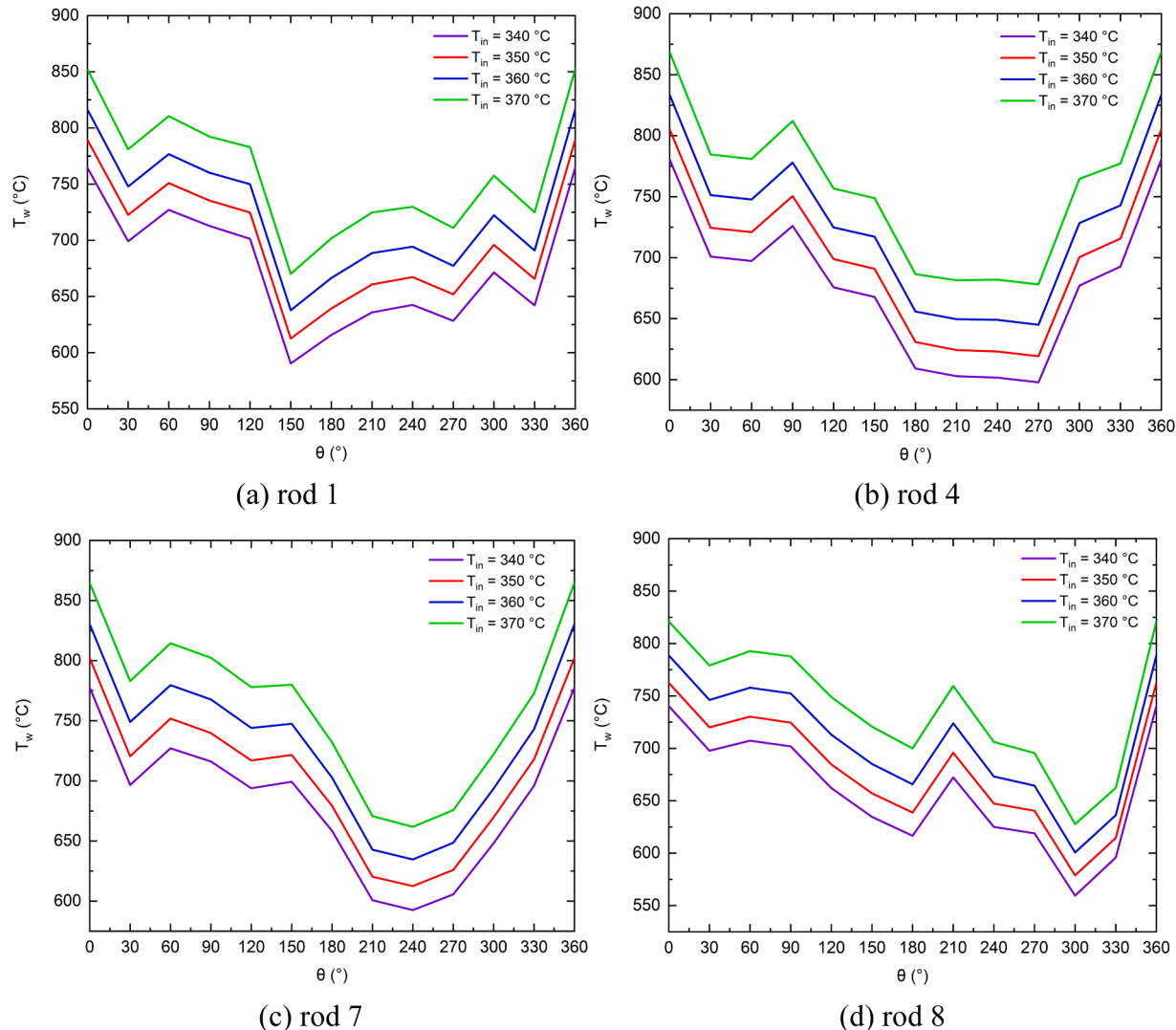


**Fig. 9.** Circumferential wall temperature distributions at  $z = 4.8$  m under different inlet temperatures.

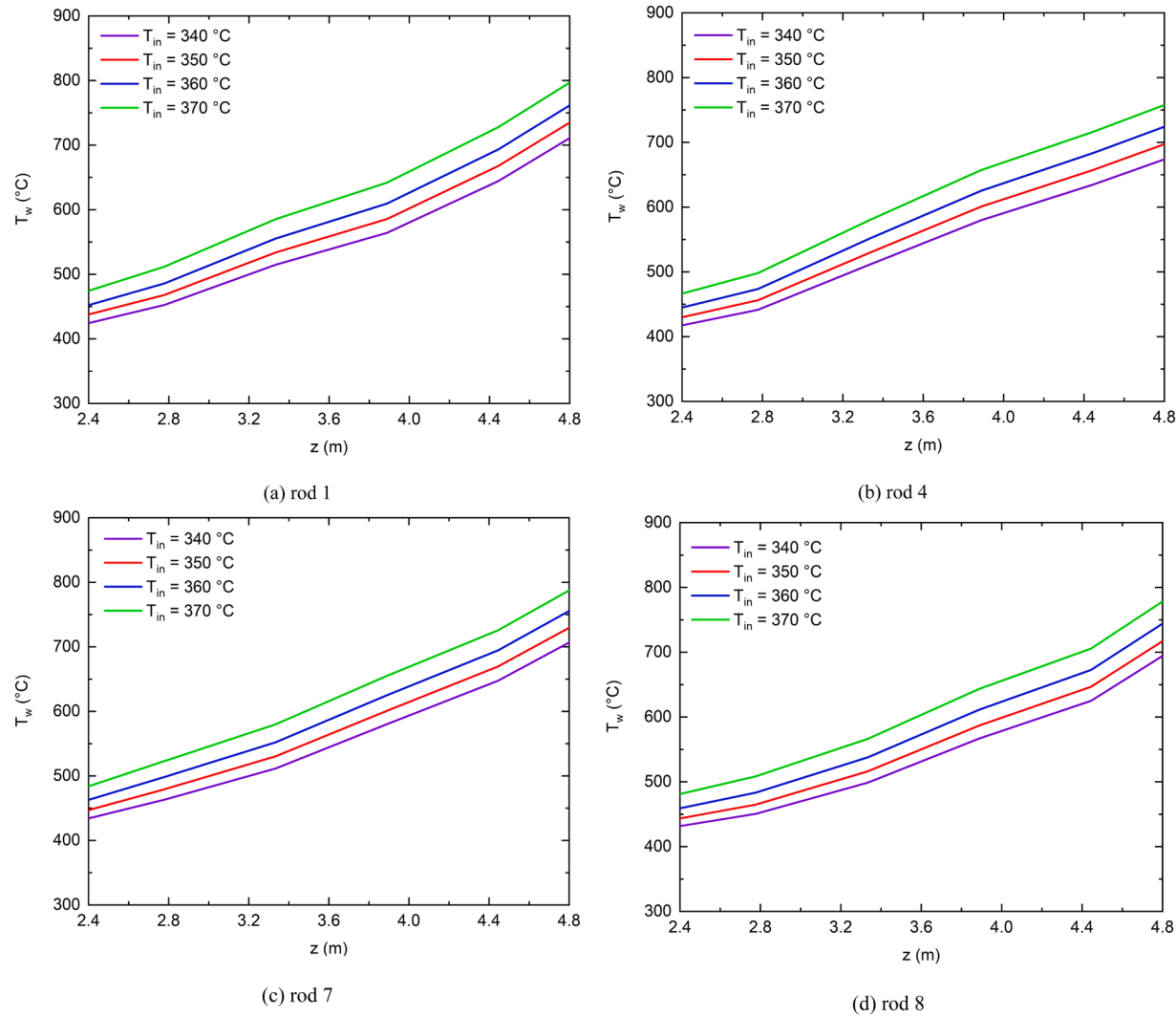


**Fig. 10.** Wall temperature distributions along the axial direction under different inlet temperatures.

circumferentially distributed in each ring [37] as shown in Fig. 2(a). The diameters of the inner and outer fuel rods are 9.5 mm and 10 mm, respectively. The supercritical water flows vertical upward in the channel. The length of the channel is 5 m. Due to the symmetry of the fuel bundle, the computational domain is reduced to a quarter of the fuel bundle to reduce the computational time, which is presented in Fig. 2(b).

The boundary conditions of the simulations are summarized here. The inlet mass flow rate and the inlet temperatures are specified as inlet boundary conditions. The outflow are used for the outlet boundary condition. At the wall, no slip and the uniform heat fluxes are specified.

## 2.2. Governing equations and turbulent models

The convective heat transfer of the supercritical water in the fuel bundle is considered as a steady state in this study. The governing equations for the three-dimensional steady state flow and heat transfer are conservations of mass, momentum and energy. They are presented as follows in the Reynolds averaged form [38]:

$$\frac{\partial \rho \bar{u}_i}{\partial x_i} = 0 \quad (1)$$

$$\frac{\partial(\rho \bar{u}_i \bar{u}_j)}{\partial x_j} = -\frac{\partial \bar{P}}{\partial x_i} + \frac{\partial}{\partial x_j} \left( \mu \frac{\partial \bar{u}_i}{\partial x_j} - \rho \bar{u}'_i \bar{u}'_j \right) + \rho g_i \quad (2)$$

$$\frac{\partial}{\partial x_i} (\bar{u}_i \rho c_p T) = \frac{\partial}{\partial x_i} \left[ \left( \lambda + \frac{c_p \mu_t}{Pr_t} \right) \frac{\partial T}{\partial x_i} \right] \quad (3)$$

The Reynolds stress model (RSM) with the variable turbulent Prandtl number ( $Pr_t$ ) proposed in the previous study [39] is used in the present work to simulate the heat transfer of the supercritical water.

The transport equations for the RSM can be described as [38]:

$$\begin{aligned} \frac{\partial}{\partial x_k} (\rho u_k \bar{u}'_i \bar{u}'_j) &= \underbrace{\frac{\partial}{\partial x_k} (\rho u_k \bar{u}'_i \bar{u}'_j)}_{C_{ij} \equiv \text{Convection}} \\ &\quad \underbrace{\frac{\partial}{\partial x_k} [\rho \bar{u}'_i \bar{u}'_j \bar{u}'_k + p' (\delta_{kj} \bar{u}'_i + \delta_{ik} \bar{u}'_j)]}_{D_{T,ij} \equiv \text{Turbulent Diffusion}} + \\ &\quad \underbrace{\frac{\partial}{\partial x_k} \left[ \mu \frac{\partial}{\partial x_k} (\bar{u}'_i \bar{u}'_j) \right]}_{D_{T,ij} \equiv \text{Molecular Diffusion}} - \underbrace{\rho \left( \bar{u}'_i \bar{u}'_k \frac{\partial u_j}{\partial x_k} + \bar{u}'_j \bar{u}'_k \frac{\partial u_i}{\partial x_k} \right)}_{P_{ij} \equiv \text{Stress Production}} - \underbrace{\rho \beta (g_i \bar{u}'_j \theta + g_j \bar{u}'_i \theta)}_{G_{ij} \equiv \sim \text{Buoyancy Production}} \\ &\quad \underbrace{p' \left( \frac{\partial u'_i}{\partial x_j} + \frac{\partial u'_j}{\partial x_i} \right)}_{\phi_{ij} \equiv \sim \text{Pressure Strain}} - \underbrace{2 \mu \frac{\partial u'_i}{\partial x_i} \frac{\partial u'_j}{\partial x_k}}_{\epsilon_{ij} \equiv \sim \text{Dissipation}} - \underbrace{2 \rho \Omega_k (\bar{u}'_i \bar{u}'_m \epsilon_{ikm} + \bar{u}'_i \bar{u}'_m \epsilon_{jkm})}_{F_{ij} \equiv \sim \text{Production by System Rotation}} + \\ &\quad \underbrace{S_{user}}_{\text{User-Defined Source Term}} \end{aligned} \quad (4)$$

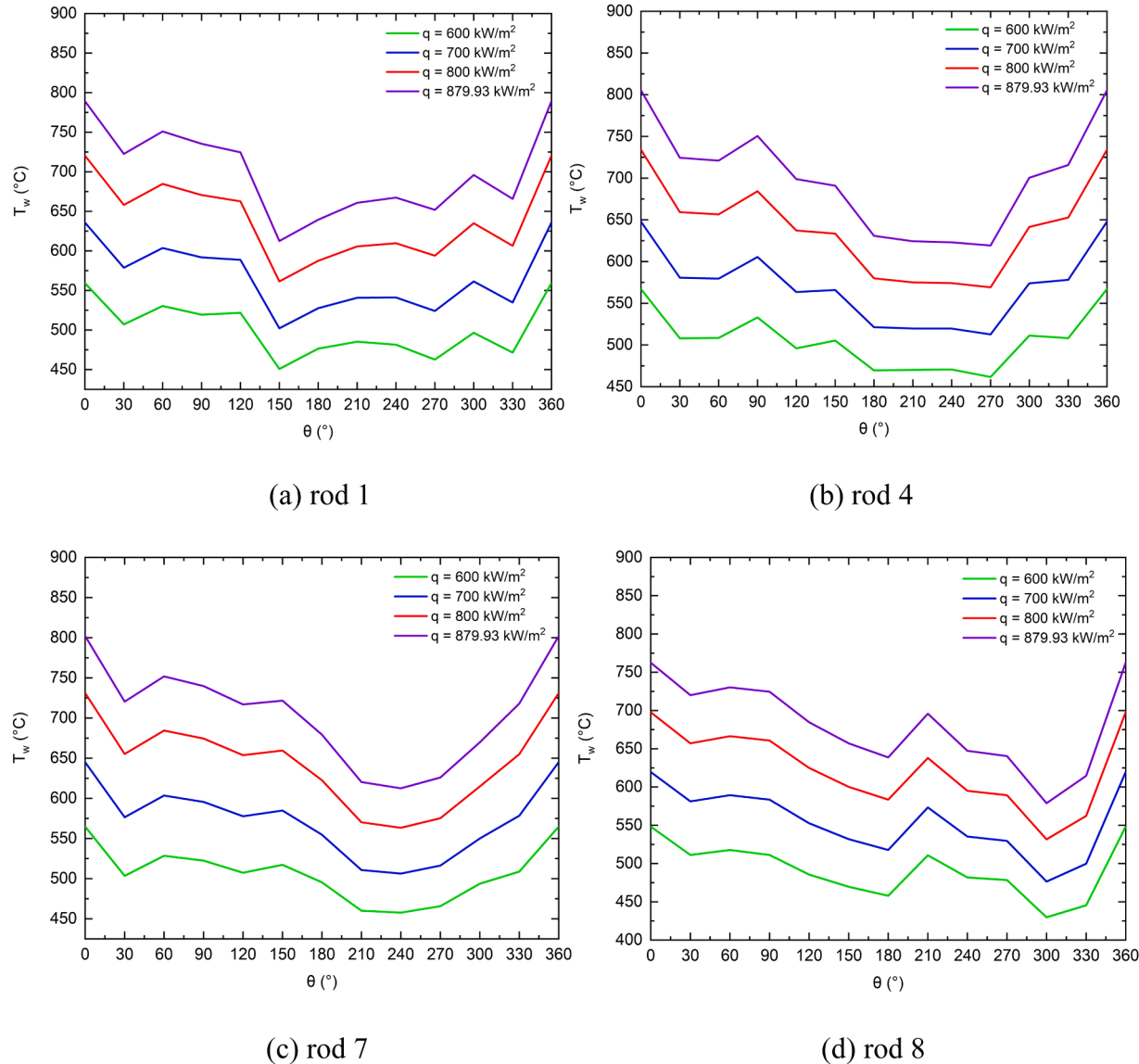


**Fig. 11.** Circumferential wall temperature distributions under different heat fluxes.

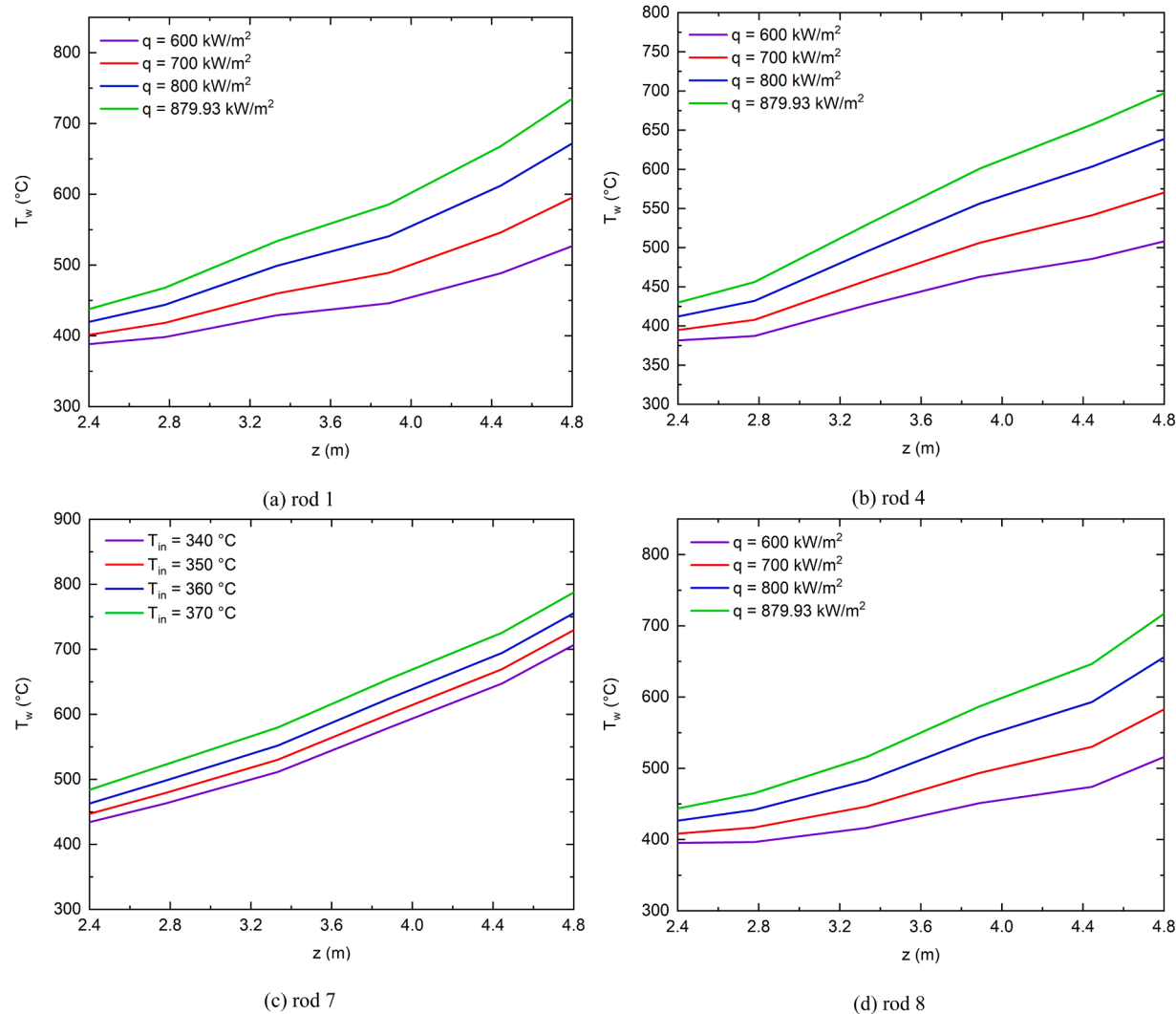


**Fig. 12.** Wall temperature distributions along the axial direction under different heat fluxes.

And  $\text{Pr}_t$  is treated as a variable and calculated as:

$$\text{Pr}_t = \begin{cases} 0.4 \frac{\mu_t}{\mu} < 0.2 \\ 0.3 + 0.03 * \frac{P}{P_{cr}} * \text{Pr} * \left( \frac{q}{G} \right) * \left( \frac{\mu_t}{\mu} \right) \quad 0.2 \leq \frac{\mu_t}{\mu} \leq 10 \\ 0.85 \frac{\mu_t}{\mu} > 10 \end{cases} \quad (5)$$

The enhanced wall treatment is used to model the near wall region and the mesh near the wall is refined to allow  $y^+$  around 1, as shown in Fig. 3. All the simulations use the mesh with 13,463,031 cells, which gives grid independent results based on previous work [40]. The finite volume method is used to solve the governing equations. The Fluent software from ANSYS is used for the simulations. The thermophysical properties of the supercritical water from the NIST standard database 9.1 [41] were implemented into the Fluent solver by using a piecewise-linear function of the temperature. The SIMPLEC scheme is used for the pressure-velocity coupling and the QUICK method is used for the discretization of the convection terms. The convergence criteria

of the residuals are set to  $10^{-6}$  to ensure sufficient accuracy. Table 2 illustrates the operating parameters of all cases for the 64-element Canadian SCWR fuel bundle in this work. The heat flux is assumed uniform for the fuel rods.

The comparison of the wall temperatures between the simulation results and experimental data by the RSM with the variable  $\text{Pr}_t$  turbulence model for the upward supercritical water flows in a bare tube (Cases # a-c) is shown in Fig. 4 and in a rod bundle (Cases # d-e) is shown in Fig. 5 [39]. The comparisons show that this turbulence model can give reasonable simulation results. Therefore, it is used in this study.

### 3. Results and discussions

#### 3.1. Bulk fluid temperature distributions under different operating conditions

Fig. 6 shows the bulk fluid temperature along the axial flow direction in the fuel bundle at different operating conditions. The axial bulk fluid

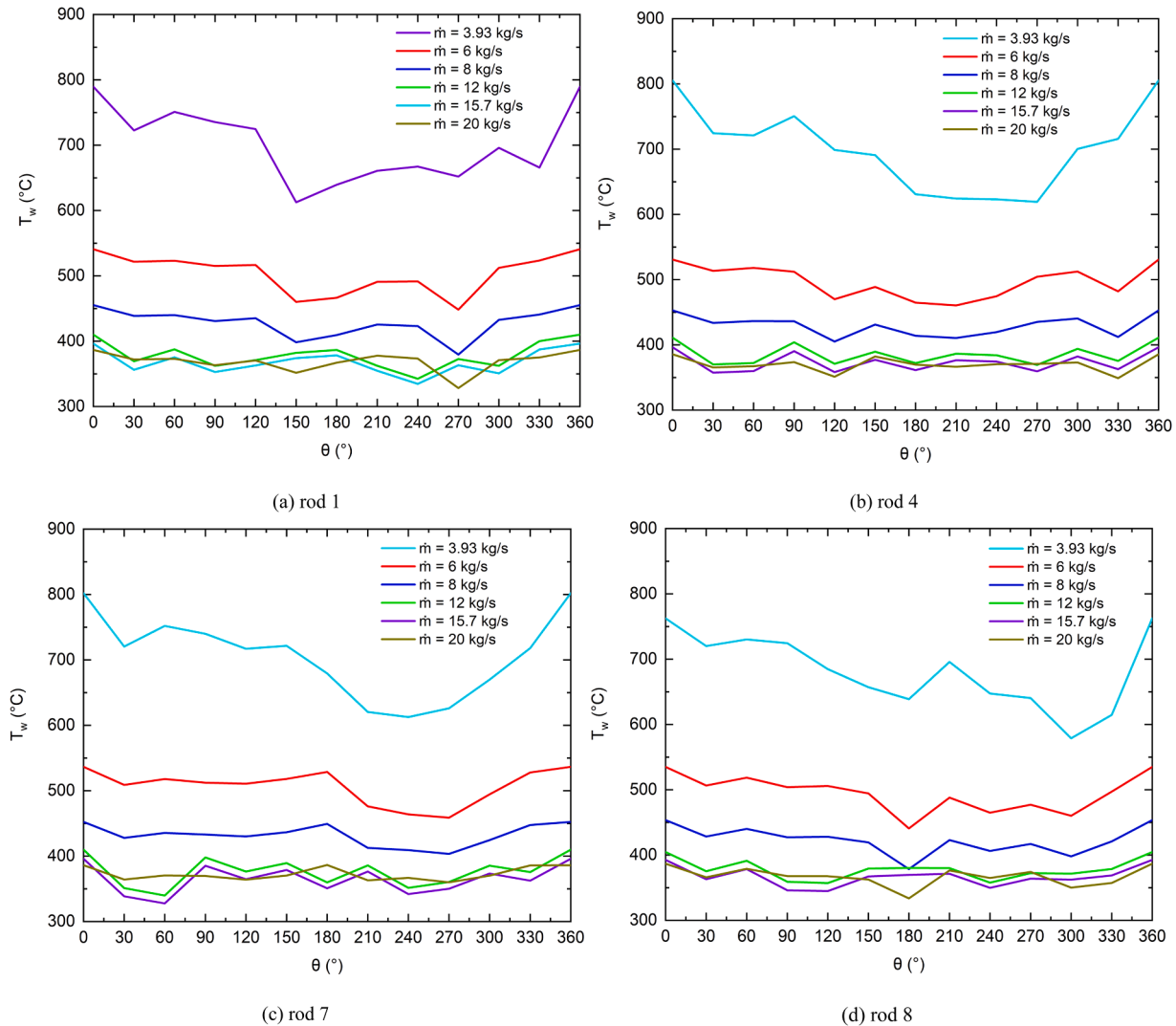


**Fig. 13.** Circumferential wall temperature distributions under different mass flow rates.

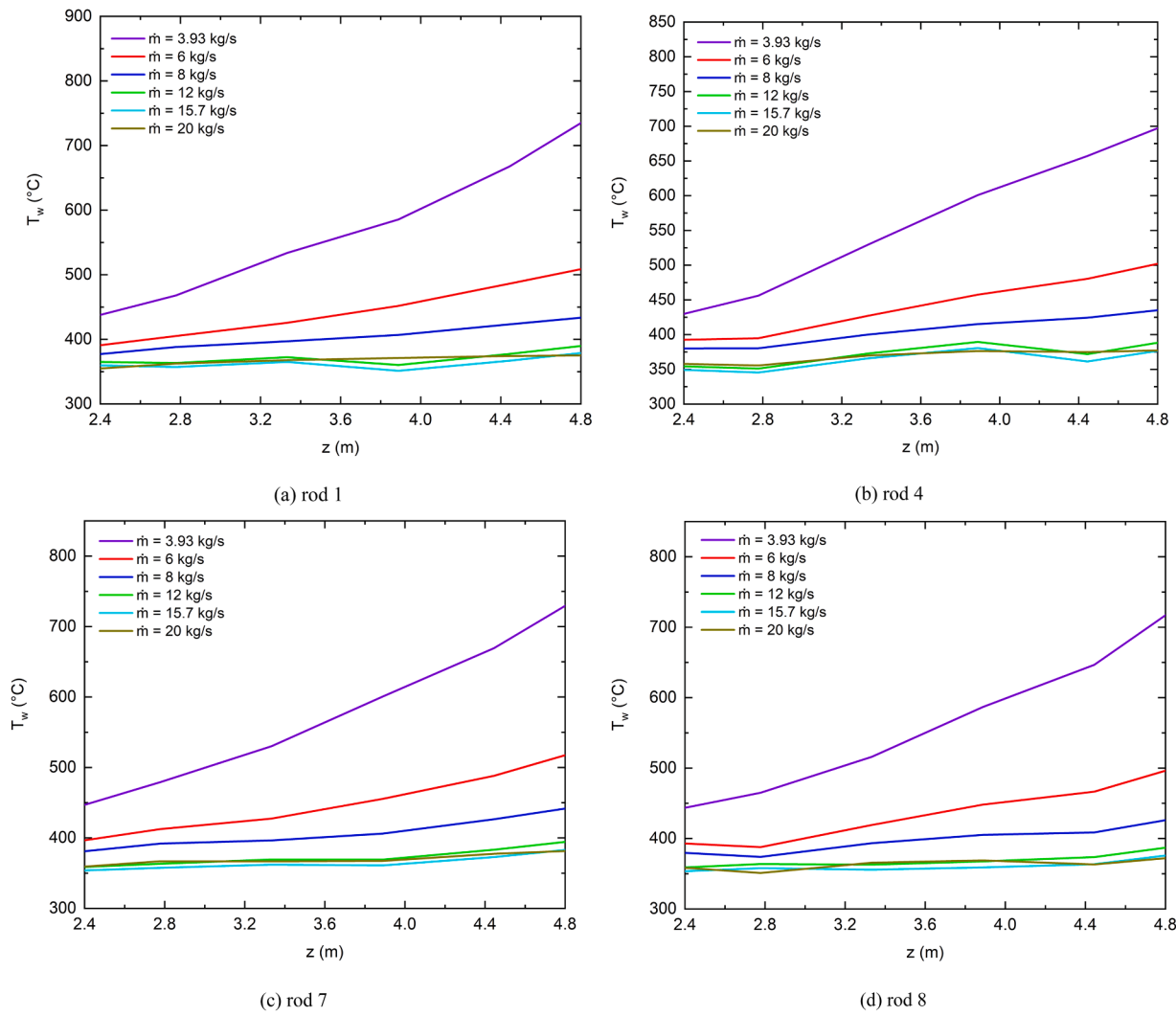


**Fig. 14.** Wall temperature distributions along the axial direction under different mass flow rates.

temperature generally increases with the increase of the inlet temperature and the heat flux, while decreases with the increase of the inlet mass flow rate. When it comes to the axial fluid temperature distribution at different operating pressures, the temperature decreases when the operating pressure increases from 25 MPa to 29 MPa, while there is little difference in the fluid temperatures at 27 MPa and 29 MPa as shown in Fig. 6(a). At the condition of 23 MPa, the variation of the fluid temperature along the axial location is much less than those at other supercritical pressure conditions. This might be due to the fact that the specific heat at  $P = 23$  MPa is more than four times higher than those at other supercritical pressure conditions when the fluid temperature is between 375°C and 380°C as shown in Fig. 1.

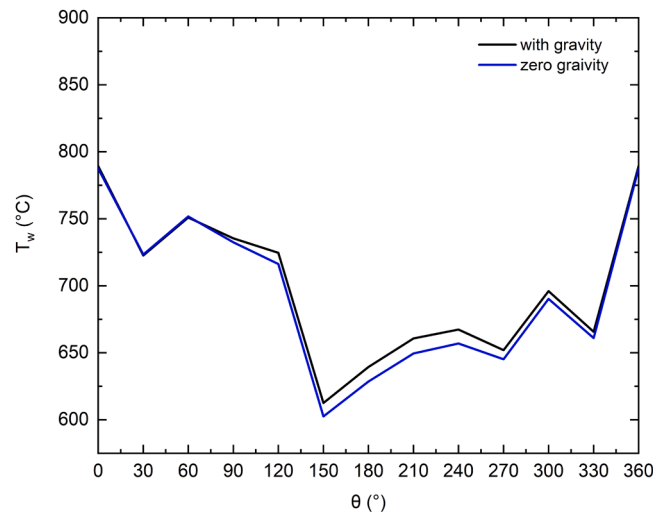
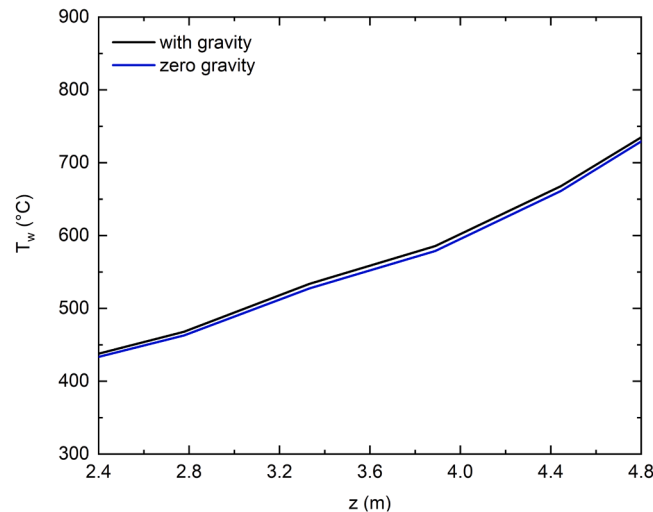
### 3.2. Effects of operation conditions on the heat transfer

To investigate the details of the heat transfer in the fuel bundle, rods #1, #4, #7, and #8 are chosen. The circumferential wall temperatures at the axial location,  $z = 4.8$  m and the axial wall temperature

distributions are presented to investigate the heat transfer in the fuel bundle.

#### 3.2.1. Effect of the operating pressure

Figs. 7 and 8 show the effect of the operating pressure on the cladding surface temperature distributions in the circumferential and axial directions, respectively. It can be seen that the wall temperature increases drastically from 370 °C to 740 °C at  $z = 4.8$  m, when the operating pressure increases from 23 MPa to 25 MPa. However, when the pressure increases from 25 MPa to 27 MPa, the wall temperature decreases from 740 °C to 575 °C at  $z = 4.8$  m. When the pressure increases further from 27 MPa to 29 MPa, the distributions of wall temperature in both circumferential and axial directions are almost the same, which might be due to the fact that the thermophysical properties of the supercritical water do not change much when the pressure is far away from the critical point.

(a) Circumferential wall temperature distribution at  $z = 4.8\text{ m}$ 

(b) Axial wall temperature distribution

**Fig. 15.** Effect of the gravity on the wall temperature of rod # 1 at the design operating condition.

### 3.2.2. Effect of the inlet temperature

The circumferential cladding surface temperature distributions at  $z = 4.8\text{ m}$  at different inlet temperatures are plotted in Fig. 9. The circumferential wall temperatures generally increase with the increase of the inlet temperature as shown in Fig. 9, as well as the axial wall temperatures, as shown in Fig. 10.

### 3.2.3. Effect of the heat flux

Variations of circumferential wall temperatures and axial wall temperatures at different heat fluxes are presented in Fig. 11 and Fig. 12, respectively. The wall temperatures increase with the increase of the heat flux.

### 3.2.4. Effect of the mass flow rate

Fig. 13 shows the circumferential wall temperature distributions at different mass flow rates. The wall temperature decreases with the increase in the mass flow rate up to  $12\text{ kg/s}$ . When the mass flow rate is higher than  $12\text{ kg/s}$ , the changes of wall temperatures are much smaller compared with those when the mass flow rate is less than  $12\text{ kg/s}$ . Similar trends of variations of wall temperatures are also observed in the axial direction, as presented in Fig. 14.

### 3.3. Effects of buoyancy on the heat transfer at different operating conditions

Fig. 15 presents the circumferential wall temperature distributions at  $z = 4.8\text{ m}$  and the axial wall temperature distributions of rod #1 at  $z = 2.4\text{--}4.8\text{ m}$  for Case #1 ( $P = 25\text{ MPa}$  and  $T_{in} = 350^\circ\text{C}$ ) at the design operating conditions of 64-element Canadian SCWR with and without considering the effect of buoyancy (gravity). It can be seen that the difference between cases with and without gravity is small. This indicates that the effect of buoyancy on the heat transfer for supercritical water in the vertical fuel rod bundle can be ignored under this operating condition.

The heat transfer in the fuel bundle flow can be mixed convection, including both natural convection and forced convection. The behavior of a natural convection process depends on the Grashof number ( $\text{Gr}$ ), which approximates the ratio of the buoyancy force to the viscous force acting on a fluid. In another aspect, the role of the Reynolds number ( $\text{Re}$ ) in the forced convection is the same as the  $\text{Gr}$  on the natural convection. When analyzing the mixed convection, the effect of the buoyancy force on the mixed convection is approximately characterized by the ratio of  $\text{Gr}$  and  $\text{Re}$ . Several criteria have been proposed in previous studies. One criterion is  $\text{Gr}/\text{Re}^2$  [42]. The effect of the buoyancy force can be ignored when  $\text{Gr}/\text{Re}^2 < 0.1$  [42–45]. Jackson and Hall [45] proposed  $\text{Gr}/\text{Re}^{2.7}$  to evaluate the effect of buoyancy force for the supercritical carbon dioxide in a vertical tube. It will be a buoyancy-free region if  $\text{Gr}/\text{Re}^{2.7} < 10^{-5}$  [46]. This criterion has been verified reliable for the upward supercritical water flow in vertical tubes [44,45,47–49]. In addition, the dimensionless parameter,  $\text{Bo}^*$  is also used to investigate the effect of the buoyancy force on the heat transfer in vertical tubes [48,50,51] and it is defined as follows:

$$\text{Bo}^* = \text{Gr} / (\text{Re}^{3.425} \text{Pr}^{0.8})$$

The effect of the buoyancy force on the heat transfer cannot be ignored when  $5.67 \times 10^{-7} < \text{Bo}^* < 8 \times 10^{-6}$ . In the present study, the above-mentioned three dimensionless parameters ( $\text{Gr}/\text{Re}^2$ ,  $\text{Gr}/\text{Re}^{2.7}$  and  $\text{Bo}^*$ ) proposed for pipe flows in the literature are used to evaluate the effect of the buoyancy force on the heat transfer at different operating conditions (Cases #1–16). The objectives are to verify whether the criteria work for the heat transfer of the supercritical water in the fuel bundle and further evaluate the effect of the buoyancy force on heat transfer of the supercritical water in the 64-element SCWR fuel bundle under different operation parameters.

Figs. 16–19 present the variations of  $\text{Gr}/\text{Re}^2$ ,  $\text{Gr}/\text{Re}^{2.7}$  and  $\text{Bo}^*$ , along the axial direction for different cases. Based on the criteria of  $\text{Gr}/\text{Re}^2$  and  $\text{Bo}^*$ , the buoyancy force effect is negligible for all cases, while based on the criterion of  $\text{Gr}/\text{Re}^{2.7}$  both buoyancy-affected and buoyancy-free zones exist along the axial direction. The buoyancy-affected zones exist at the entrance region for all operating parameters. As seen from Fig. 16(b), the buoyancy-affected zone is at around  $z = 0\text{--}1\text{ m}$  for all pressures (23–29 MPa). This is due to the sharp

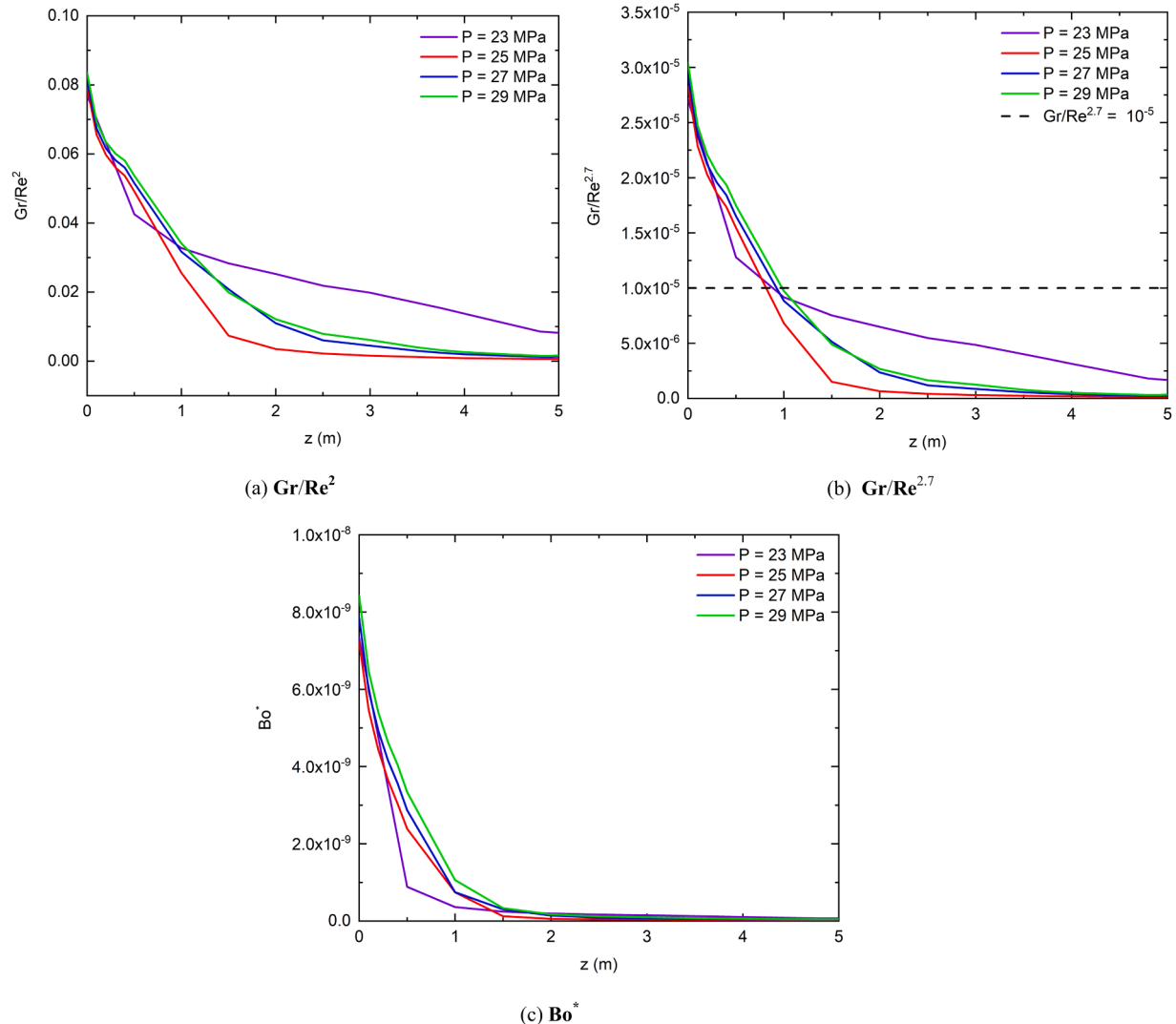


**Fig. 16.** Variations of  $\text{Gr}/\text{Re}^2$ ,  $\text{Gr}/\text{Re}^{2.7}$  and  $\text{Bo}^*$  along the axial direction at different pressures.

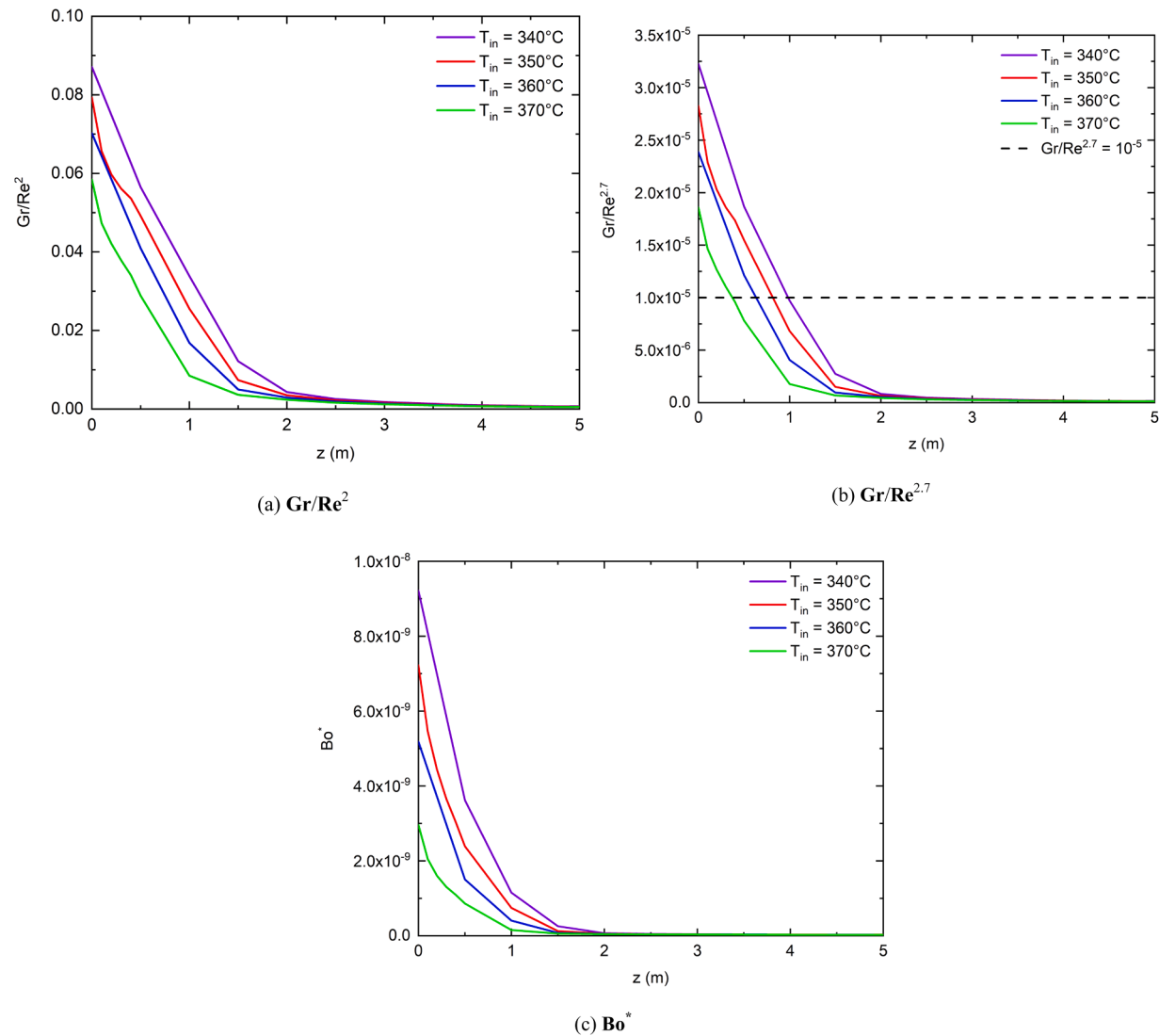


**Fig. 17.** Variations of  $\text{Gr}/\text{Re}^2$ ,  $\text{Gr}/\text{Re}^{2.7}$  and  $\text{Bo}^*$  along the axial direction at different inlet temperatures.

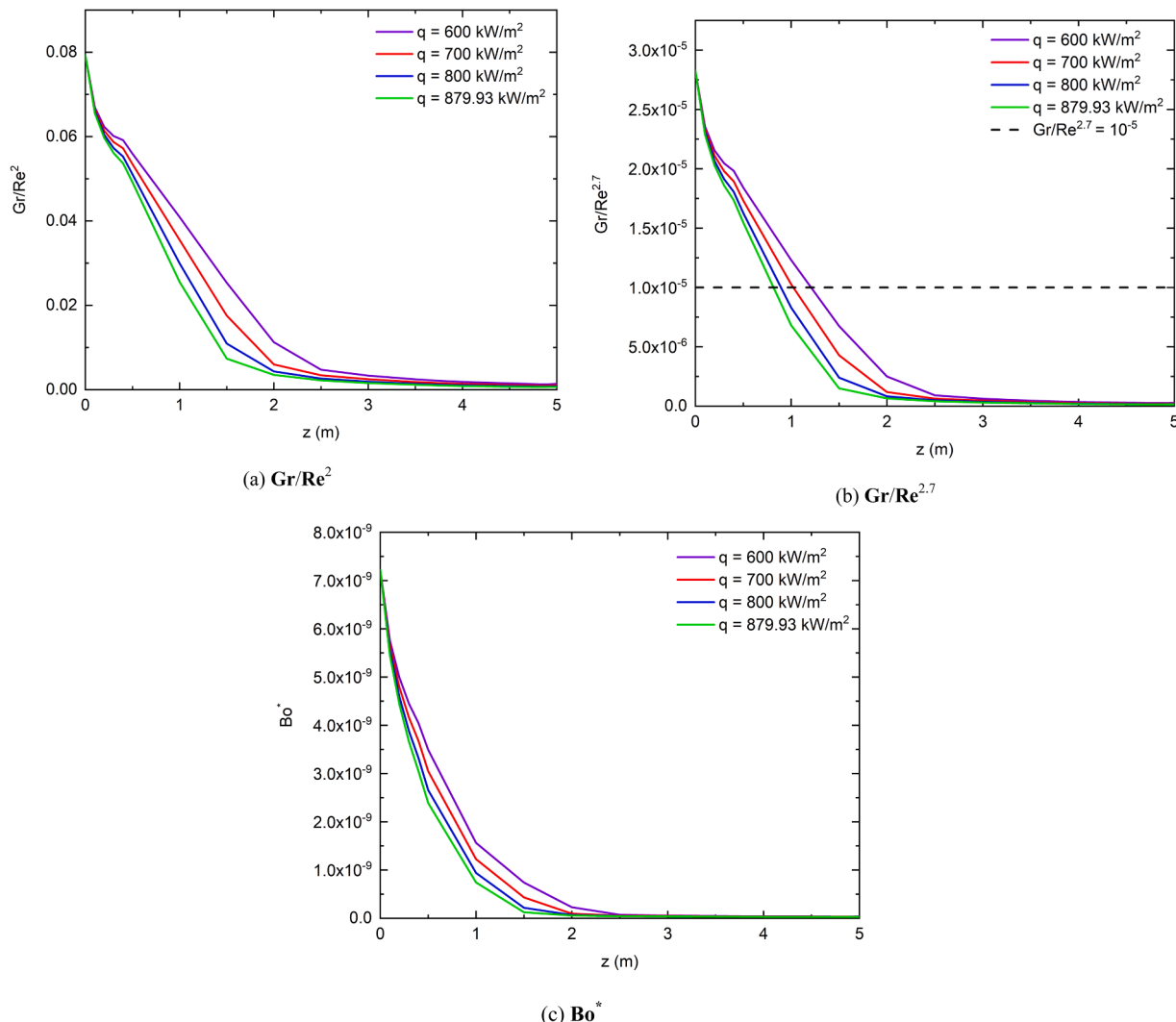


**Fig. 18.** Variations of  $\text{Gr}/\text{Re}^2$ ,  $\text{Gr}/\text{Re}^{2.7}$  and  $\text{Bo}^*$  along the axial direction at different heat fluxes.

decrease of the density at around  $z = 0\text{--}1$  m, as shown in Fig. 1. Figs. 17b and 18(b) show that with the increase of the inlet temperature and the heat flux, the buoyancy-affected zone is reduced. It is reasonable because the pseudocritical region where the gradient of density is large is narrowed with the increase of the inlet temperature and heat flux. Results shown in Fig. 19(b) indicate that the buoyancy effect on the heat transfer of the supercritical water in the fuel bundle can be ignored when the mass flow rate is greater than 6 kg/s.

#### 4. Conclusions

The heat transfer of the supercritical water was investigated in the 64-element Canadian SCWR fuel bundle under different operating conditions using previously validated RSM with the variable  $\text{Pr}_t$ . The effects of the operating pressure, inlet temperature, heat flux, mass flux were analyzed. The wall temperature generally increases with the increase in the inlet temperature, increase in the heat flux, or decrease in the mass

flux. When the operating pressure is away from the critical pressure, the wall temperatures does not change much with the change of pressure. Since the buoyancy effect contributes to the heat transfer deterioration, several criteria in the literature for evaluating the buoyancy effects for supercritical water flow in heated tube,  $\text{Gr}/\text{Re}^2$ ,  $\text{Gr}/\text{Re}^{2.7}$ , and  $\text{Bo}^*$ , were also examined in this study. These criteria for the supercritical water in the 64-element SCWR fuel bundle at different operating conditions were compared and discussed. Based on the criteria  $\text{Gr}/\text{Re}^2$  and  $\text{Bo}^*$ , there is no buoyancy-affected region under all operating conditions considered in this study. Based on the criterion  $\text{Gr}/\text{Re}^{2.7}$ , the buoyancy-affected zones exist at the entrance region ( $z = 0\text{--}1$  m) where the fluid bulk temperature ( $T_b$ ) is close to the pseudocritical temperature ( $T_{pc}$ ) and other regions along the axial direction are buoyancy-free zones where  $T_b > T_{pc}$  at all pressures (23–29 MPa). With the increase of the inlet temperature and the heat flux, the buoyancy-affected zone is reduced. The results for different mass fluxes indicate that the buoyancy effect on heat transfer of the supercritical water in the fuel bundle is

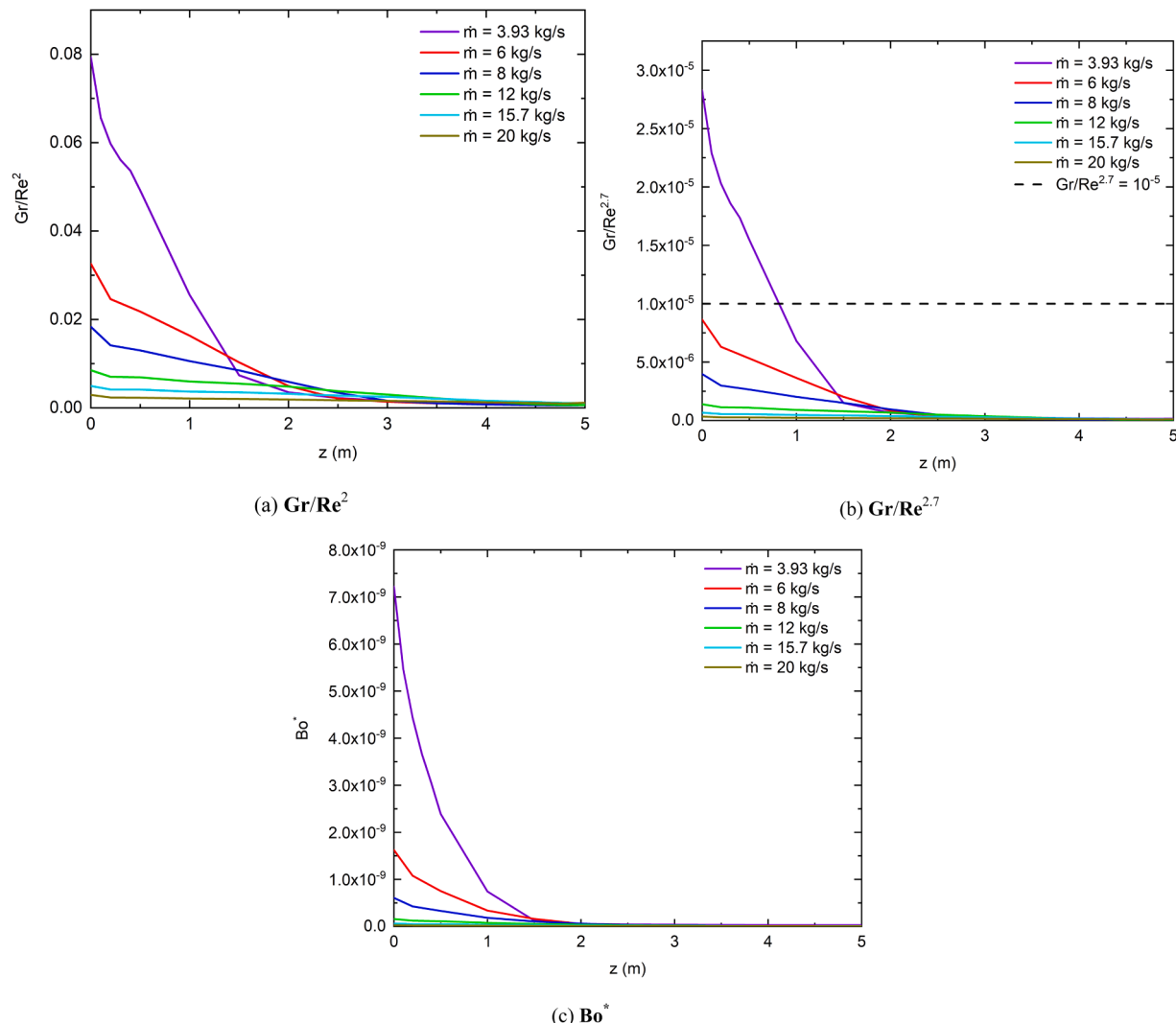


**Fig. 19.** Variations of  $\text{Gr}/\text{Re}^2$ ,  $\text{Gr}/\text{Re}^{2.7}$  and  $\text{Bo}^*$  along the axial direction at different mass flow rates.

negligible when the mass flow rate is greater than 6 kg/s.

#### Declaration of Competing Interest

The authors declare that they have no known competing financial interests or personal relationships that could have appeared to influence the work reported in this paper.

#### Data availability

Data will be made available on request.

#### Acknowledgements

This work was supported by the Natural Sciences and Engineering Research Council of Canada (NSERC) Discovery grant [grant number #04757].

#### References

- [1] M. Shitsman, Impairment of the heat transmission at supercritical pressures, *High. Temp.* 1 (1963) 237–244. (<http://mi.mathnet.ru/eng/tvt/v1/i2/p267>).
- [2] H.S. Swenson, J. Carver, C.R. Kakarala, Heat transfer to supercritical water in smooth-bore tubes, *J. Heat. Transf.* 87 (4) (1965) 477–483, <https://doi.org/10.1115/1.3689139>.
- [3] B. Shiralkar, P. Griffith, Deterioration in heat transfer to fluids at supercritical pressure and high heat fluxes, *J. Heat. Transf.* 91 (1) (1969) 27–36, <https://doi.org/10.1115/1.3580115>.
- [4] A.P. Ornatskij, L.F. Glushchenko, S.I. Kalachev, Heat transfer with rising and falling flows of water in tubes of small diameter at supercritical pressures, *Therm. Eng.* 18 (5) (1971) 137–141.
- [5] K. Yamagata, K. Nishikawa, S. Hasegawa, T. Fujii, S. Yoshida, Forced convective heat transfer to supercritical water flowing in tubes, *Int. J. Heat. Mass. Transf.* 15 (12) (1972) 2575–2593, [https://doi.org/10.1016/0017-9310\(72\)90148-2](https://doi.org/10.1016/0017-9310(72)90148-2).
- [6] I. Pioro, S. Mokry, Thermophysical properties at critical and supercritical pressures. in: *Heat Transfer - Theoretical Analysis, Experimental Investigations and Industrial Systems*, InTech, 2011, pp. 573–592.
- [7] OECD Nuclear Energy Agency, Technology roadmap update for generation IV nuclear energy systems, in: *Proceedings of the Gen IV Int. Forum*, 2014, 1–66, .
- [8] S. Koshizuka, N. Takano, Y. Oka, Numerical analysis of deterioration phenomena in heat transfer to supercritical water, *Int. J. Heat. Mass. Transf.* 38 (16) (1995) 3077–3084, [https://doi.org/10.1016/0017-9310\(95\)00008-W](https://doi.org/10.1016/0017-9310(95)00008-W).
- [9] S.H. Lee, J.R. Howell, Turbulent developing convective heat transfer in a tube for fluids near the critical point, *Int. J. Heat. Mass. Transf.* 41 (10) (1998) 1205–1218, [https://doi.org/10.1016/S0017-9310\(97\)00217-2](https://doi.org/10.1016/S0017-9310(97)00217-2).
- [10] Y. Zhang, C. Zhang, J. Jiang, Numerical simulation of fluid flow and heat transfer of supercritical fluids in fuel bundles, *J. Nucl. Sci. Technol.* 48 (6) (2011) 929–935, <https://doi.org/10.1080/18811248.2011.9711779>.
- [11] H. Wang, S. Wang, D. Lu, Large eddy simulation on the heat transfer of supercritical pressure water in a circular pipe, *Nucl. Eng. Des.* 377 (2021), 111146, <https://doi.org/10.1016/j.nucengdes.2021.111146>.
- [12] S. Yu, H. Li, X. Lei, Y. Feng, Y. Zhang, H. He, T. Wang, Experimental investigation on heat transfer characteristics of supercritical pressure water in a horizontal tube, *Exp. Therm. Fluid Sci.* 50 (2013) 213–221, <https://doi.org/10.1016/j.expthermflusci.2013.06.011>.
- [13] X. Lei, H. Li, W. Zhang, N.T. Dinh, Y. Guo, S. Yu, Experimental study on the difference of heat transfer characteristics between vertical and horizontal flows of

- supercritical pressure water, *Appl. Therm. Eng.* 113 (2017) 609–620, <https://doi.org/10.1016/j.applthermaleng.2016.11.051>.
- [14] X. Lei, H. Li, N. Dinh, W. Zhang, A study of heat transfer scaling of supercritical pressure water in horizontal tubes, *Int. J. Heat. Mass Transf.* 114 (2017) 923–933, <https://doi.org/10.1016/j.ijheatmasstransfer.2017.06.052>.
- [15] H. Wang, Q. Bi, L. Wang, H. Lv, L.K.H. Leung, Experimental investigation of heat transfer from a  $2 \times 2$  rod bundle to supercritical pressure water, *Nucl. Eng. Des.* 275 (2014) 205–218, <https://doi.org/10.1016/j.nucengdes.2014.04.036>.
- [16] V.I. Deev, V.S. Kharitonov, A.M. Baisov, A.N. Churkin, Heat transfer in rod bundles cooled by supercritical water – experimental data and correlations, *Therm. Sci. Eng. Prog.* 15 (2020), <https://doi.org/10.1016/j.tssep.2019.100435>.
- [17] H. Wang, Q. Bi, L.K.H. Leung, Heat transfer from a  $2 \times 2$  wire-wrapped rod bundle to supercritical pressure water, *Int. J. Heat. Mass Transf.* 97 (2016) 486–501, <https://doi.org/10.1016/j.ijheatmasstransfer.2016.02.036>.
- [18] W. Gang, Q. Bi, Z. Yang, H. Wang, X. Zhu, H. Hao, L.K.H. Leung, Experimental investigation of heat transfer for supercritical pressure water flowing in vertical annular channels, *Nucl. Eng. Des.* 241 (9) (2011) 4045–4054, <https://doi.org/10.1016/j.nucengdes.2011.07.007>.
- [19] J. Wang, H. Li, S. Yu, T. Chen, Investigation on the characteristics and mechanisms of unusual heat transfer of supercritical pressure water in vertically-upward tubes, *Int. J. Heat. Mass Transf.* 54 (9–10) (2011) 1950–1958, <https://doi.org/10.1016/j.ijheatmasstransfer.2011.01.008>.
- [20] X. Zhu, Q. Bi, D. Yang, T. Chen, An investigation on heat transfer characteristics of different pressure steam-water in vertical upward tube, *Nucl. Eng. Des.* 239 (2) (2009) 381–388, <https://doi.org/10.1016/j.nucengdes.2008.10.026>.
- [21] K. Podila, Y.F. Rao, CFD analysis of flow and heat transfer in Canadian supercritical water reactor bundle, *Ann. Nucl. Energy* 75 (2014) 1–10, <https://doi.org/10.1016/j.anucene.2014.07.039>.
- [22] I.L. Pioro, R.B. Duffey, *Heat Transfer and Hydraulic Resistance at Supercritical Pressures in Power Engineering Applications*, ASME Press, New York, NY, USA, 2007.
- [23] S. Mokry, I. Pioro, A. Farah, K. King, S. Gupta, W. Peiman, P. Kirillov, Development of supercritical water heat-transfer correlation for vertical bare tubes, *Nucl. Eng. Des.* 241 (4) (2011) 1126–1136, <https://doi.org/10.1016/j.nucengdes.2010.06.012>.
- [24] L. Liu, Z. Xiao, X. Yan, X. Zeng, Y. Huang, Heat transfer deterioration to supercritical water in circular tube and annular channel, *Nucl. Eng. Des.* 255 (2013) 97–104, <https://doi.org/10.1016/j.nucengdes.2012.09.025>.
- [25] M. Zhao, H.Y. Gu, X. Cheng, Experimental study on heat transfer of supercritical water flowing downward in circular tubes, *Ann. Nucl. Energy* 63 (2014) 339–349, <https://doi.org/10.1016/j.anucene.2013.07.003>.
- [26] W. Wang, L. Guo, G. Zhu, X. Zhu, Q. Bi, Experimental investigation on heat transfer of supercritical water flowing in the subchannel with grid spacer in supercritical water-cooled reactor, *Energies* 13 (5) (2020), <https://doi.org/10.3390/en13051016>.
- [27] M. Zhao, H.Y. Gu, Experimental and numerical investigation on heat transfer of supercritical water flowing upward in  $2 \times 2$  rod bundles, *Nucl. Eng. Des.* 370 (October) (2020), 110903, <https://doi.org/10.1016/j.nucengdes.2020.110903>.
- [28] X. Hao, P. Xu, H. Suo, L. Guo, Numerical investigation of flow and heat transfer of supercritical water in the water-cooled wall tube, *Int. J. Heat. Mass Transf.* 148 (2020), 119084, <https://doi.org/10.1016/j.ijheatmasstransfer.2019.119084>.
- [29] R. Maitri, H. Han, C. Zhang, J. Jiang, Numerical investigation of the deteriorated heat transfer phenomenon for supercritical water flows in vertical circular tubes, in: A. Vasel-Be-Hagh, D.S.-K. Ting (Eds.), in: *Complementary Resources for Tomorrow*, Springer International Publishing, Cham, 2020, pp. 235–248, [https://doi.org/10.1007/978-3-030-38804-1\\_15](https://doi.org/10.1007/978-3-030-38804-1_15).
- [30] H.Y. Gu, Z.X. Hu, D. Liu, H.B. Li, M. Zhao, X. Cheng, Experimental study on heat transfer to supercritical water in  $2 \times 2$  rod bundle with wire wraps, *Exp. Therm. Fluid Sci.* 70 (2016) 17–28, <https://doi.org/10.1016/j.expthermflusci.2015.08.015>.
- [31] W. Zhang, H. Li, Q. Zhang, X. Lei, Q. Zhang, Experimental investigation on heat transfer deterioration of supercritical pressure water in vertically-upward internally-ribbed tubes, *Int. J. Heat. Mass Transf.* 120 (2018) 930–943, <https://doi.org/10.1016/j.ijheatmasstransfer.2017.12.097>.
- [32] H. Han, C. Zhang, Numerical simulation of fluid flow and heat transfer of the supercritical water in different fuel rod channels, in: *Progress in Canadian Mechanical Engineering*, 2018. <https://doi.org/10.25071/10315/35367>.
- [33] X. Lei, Y. Guo, W. Zhang, H. Li, L. Li, Development of heat transfer correlation for supercritical water in vertical upward tubes, *Heat. Transf. Eng.* 40 (8) (2019) 652–666, <https://doi.org/10.1080/01457632.2018.1436656>.
- [34] F. Yin, T.-K. Chen, H.-X. Li, An investigation on heat transfer to supercritical water in inclined upward smooth tubes, *Heat. Transf. Eng.* 27 (9) (2006) 44–52, <https://doi.org/10.1080/01457630600846018>.
- [35] V.A. Grabezhnaya, P.L. Kirillov, Heat transfer under supercritical pressures and heat transfer deterioration boundaries, *Therm. Eng.* 53 (4) (2006) 296–301, <https://doi.org/10.1134/S0040601506040069>.
- [36] M.T. Kao, M. Lee, Y.M. Ferng, C.C. Chieng, Heat transfer deterioration in a supercritical water channel, *Nucl. Eng. Des.* 240 (10) (2010) 3321–3328, <https://doi.org/10.1016/j.nucengdes.2010.06.028>.
- [37] M. Yetisir, H. Hamilton, R. Xu, M. Gaudet, D. Rhodes, M. King, K. Andrew, B. Benson, Fuel assembly concept of the canadian supercritical water-cooled reactor, *J. Nucl. Eng. Radiat. Sci.* 4 (1) (2018) 1–7, <https://doi.org/10.1115/1.4037818>.
- [38] ANSYS, Ansys Fluent Theory Guide, 2013.
- [39] H. Han, C. Zhang, A modified turbulent model for the supercritical water flows in the vertical upward channels, *J. Supercrit. Fluids* (2022), 105632, <https://doi.org/10.1016/j.supflu.2022.105632>.
- [40] H. Han , C. Zhang, Numerical Simulation of Fluid Flow and Heat Transfer of the Supercritical Water in the 64-Element Canadian SCWR Fuel Bundle,(Submitted).
- [41] E. Lemmon, M. Huber, M. McLinden, 2013. NIST Reference Fluid Thermodynamic and Transport Properties-RFFPROP, VErsion 9.1. National Institute of Standard Technology, 2013.
- [42] B. Metais, E.R.G. Eckert, Forced, mixed, and free convection regimes, *J. Heat. Transf.* 86 (2) (1964) 295–296, <https://doi.org/10.1115/1.3687128>.
- [43] F.P. Incropera, *Fundamentals of Heat and Mass Transfer*, sixth ed., John Wiley, Hoboken, NJ, 2007.
- [44] B. Zhang, J. Shan, J. Jiang, Numerical analysis of supercritical water heat transfer in horizontal circular tube, *Prog. Nucl. Energy* 52 (7) (2010) 678–684, <https://doi.org/10.1016/j.pnucene.2010.03.006>.
- [45] Z. Gao, J. Bai, Numerical analysis on nonuniform heat transfer of supercritical pressure water in horizontal circular tube, *Appl. Therm. Eng.* 120 (2017) 10–18, <https://doi.org/10.1016/j.applthermaleng.2017.03.109>.
- [46] J.D. Jackson , W.B. Hall, Influences of Buoyancy on Heat Transfer to Fluids Flowing in Vertical Tubes Under Turbulent Conditions, 1979.
- [47] A. Bruch, A. Bontemps, S. Colasson, Experimental investigation of heat transfer of supercritical carbon dioxide flowing in a cooled vertical tube, *Int. J. Heat. Mass Transf.* 52 (11–12) (2009) 2589–2598, <https://doi.org/10.1016/j.ijheatmasstransfer.2008.12.021>.
- [48] J. Guo, M. Xiang, H. Zhang, X. Huai, K. Cheng, X. Cui, Thermal-hydraulic characteristics of supercritical pressure CO<sub>2</sub> in vertical tubes under cooling and heating conditions, *Energy* 170 (2019) 1067–1081, <https://doi.org/10.1016/j.energy.2018.12.177>.
- [49] R. Peng, X. Lei, Z. Guo, Y. Wang, H. Li, X. Zhou, Forced convective heat transfer of supercritical carbon dioxide in mini-channel under low mass fluxes, *Int. J. Heat. Mass Transf.* 182 (2022), 121919, <https://doi.org/10.1016/j.ijheatmasstransfer.2021.121919>.
- [50] J.D. Jackson, M.A. Cotton, B.P. Axcell, Studies of mixed convection in vertical tubes, *Int. J. Heat. Fluid Flow*. 10 (1) (1989) 2–15, [https://doi.org/10.1016/0142-727X\(89\)90049-0](https://doi.org/10.1016/0142-727X(89)90049-0).
- [51] D.P. Mikielewicz, A.M. Shehata, J.D. Jackson, D.M. McEligot, Temperature, velocity and mean turbulence structure in strongly heated internal gas flows: comparison of numerical predictions with data, *Int. J. Heat. Mass Transf.* 45 (21) (2002) 4333–4352, [https://doi.org/10.1016/S0017-9310\(02\)00119-9](https://doi.org/10.1016/S0017-9310(02)00119-9).